# Titanium-Based Metal-Organic Frameworks for Photocatalytic Applications

Jianjun Zhu[a,b,d], Pei-Zhou Li[a,d], Wenhan Guo[c,d], Yanli Zhao[a,*], Ruqiang Zou[c,*]

[a] *Division of Chemistry and Biological Chemistry, School of Physical and Mathematical Sciences, Nanyang Technological University, 21 Nanyang Link 637371, Singapore*

[b] *Henan Province Key Laboratory of Utilization of Non-metallic Mineral in the South of Henan, College of Chemistry and Chemical Engineering, Xinyang Normal University, Xinyang 464000, China*

[c] *Beijing Key Laboratory for Theory and Technology of Advanced Battery Materials, Department of Materials Science and Engineering, College of Engineering, Perking University, Beijing 100871, China*

[d] *J Zhu, P Li, and W Guo contributed equally to this work.*

## ABSTRACT

Titanium-based metal-organic frameworks (Ti-MOFs) are considered one of the most appealing subclasses of the MOFs family owing to their promising optoelectronic and photocatalytic properties, high thermal and chemical stability, and unique structural features. Restricted by their challenging synthesis, however, only limited Ti-MOFs have been reported and utilized so far. In this review, we comprehensively summarize the synthesis, structures

Abbreviations: AB, ammonia borane; abz, 4-aminobenzoate; AC, acetylacetone; BDA, benzene-1,4-dialdehyde; BET, Brunauer-Emmett-Teller; BMA, benzyl methacrylate; BPDA, 4,4'-biphenyldicarboxaldehyde; cat, catecholate; cdc, *trans*-1,4-cyclo-hexanedicarboxylate; COFs, covalent-organic frameworks; CPE, carbon paste electrode; [$Cp_2Ti^{IV}Cl_2$], dicyclopentadienyl titanium(IV) dichloride; CTAB, cetyltrimethylammonium bromide; dabco, 1,4-diazabicyclo-[2.2.2]octane; DEAH, diethylammonium; DEF, N,N'-diethylformamide; DMF, N,N'-dimethylformamide; dmobpy, 4,4'-dimethoxy-2,2'-bipyridine; DSSC, dye-sensitized solar cell; EXAFS, Extended X-ray Absorption Fine Structure; GFs, graphite felts; $H_2$cdc, *trans*-1,4-cyclo-hexanedicarboxylic acid; $H_3$obdc, 2-hydroxyterephthalic acid; $H_3$ondc, 3-hydroxy-2,7-naphthalenedicarboxylic acid; $H_4$DOBDC, 2,5-dihydroxyterephthalic acid; $H_4$L, N,N'-piperazinebismethylenephosphonic acid; $H_6$THO, 2,3,6,7,9,11-hexahydroxytriphenylene; HVMO, high valence metathesis and oxidation; LIBs, lithium ion batteries; LMCT, ligand-to-metal charge transfer; LUMO, Lowest Unoccupied Molecular Orbital; MB, methylene blue; MMA, methyl methacrylate; MOFs, metal-organic frameworks; MOPs, metal-organic polyhedrons; NDC, 2,6-naphthalen-di-carboxylate; NIBs, Na ion batteries; NMR, Nuclear Magnetic Resonance; NTU, Nanyang Technological University; pip$H_2$, piperazinium; PSM, post-synthetic metathesis; PXRD, powder X-ray diffraction; P123, PEG-PPG-PEG symmetric triblock copolymer; RFB, redox flow battery; rGO, reduced graphene oxide; RhB, rhodamine B; RSD, relative standard deviation; SBUs, secondary building blocks; TBOT, tetrabutyl titanate; TCPP, tetrakis(4-carboxyphenyl) porphyrin; TEOA, triethanolamine; Ti(iOPr)$_4$, Titanium tetraisopropoxide; Ti-MOFs, Titanium-based metal-organic frameworks; Ti(OR)$_4$, Titanium alkoxides; TOF, turn-over frequency; TON, turn-over number; UV, Ultraviolet; VAC, vapor-assisted crystallization; Vis-IR, visible-infrared; Vis-NIR, visible-near infrared; XRD, X-ray diffraction; 2D, bidimensional; 2-mpy, 2-mercapto-pyridyl;3D, tridimensional.

* Corresponding authors.

*E-mail addresses:* rzou@pku.edu.cn (Ruqiang Zou), zhaoyanli@ntu.edu.sg (Yanli Zhao).

and photocatalytic applications of Ti-MOFs reported to date, particularly focusing on the synthetic strategy to develop new Ti-MOF structures and composites as photocatalysts with high sunlight harvesting efficiency and photocatalytic activity. Photocatalytic applications including photocatalytic redox reactions, water splitting, organic pollutant degradation, polymerization, deoximation reaction and sensors are highlighted. For wider interests, other applications of Ti-MOFs are also briefly introduced. This review aims to provide up-to-date developments of Ti-MOFs beneficial to researchers who currently work or are interested in this field.

***Keywords:*** metal-organic frameworks • photocatalysis • porous materials • structure • titanium

**Contents**

## 1. Introduction

Metal-organic frameworks (MOFs) have welcomed their third decade of intensive study since the early 1990s [1-4]. During the last 20 years, the MOF community has been significantly developed, attracting researchers from diverse fields including coordination chemistry [5-7], nano-engineering [8-10], gas storage and separation [11-16], catalysis [17-23], optics and optoelectronics [24-28], sensing [29-31], energy storage and conversion [32-35], biomedical science [36-39] etc. In terms of the chemistry nature of MOFs, one of the

ultimate purposes of structural chemists is to construct MOFs from any metallic element in the periodic table in a well-controlled and pre-designed manner. Such efforts have partially succeeded considering the thousands of MOFs reported hitherto, mostly constructed from di- or trivalent ions of 3p metals [40], 3d transition metals [41-44] and lanthanides [45, 46], while developing MOFs based on high-valent metal ions remains a big challenge [47, 48]. On the other hand, increasing the charge of metal ions leads to stronger polarizing power, which significantly strengthens the metal-ligand bonds and hence improves the chemical stability of MOFs [49]. Most of the MOFs constructed from divalent metal ions ($Zn^{2+}$, $Co^{2+}$, $Ni^{2+}$, $Cu^{2+}$, etc.) including many highly porous and conventional ones (MOF-5, MOF-74, HKUST-1, etc.) suffer from poor water stability due to weak interaction between metal centers and organic ligands, limiting their wide applications [50-54]. Trivalent ions ($Fe^{3+}$, $Al^{3+}$, $Cr^{3+}$, etc.) have proven useful in building MOFs with high stability [55, 56], and the success of Zr-based MOFs, started from the prototypical UiO-66 [57], undoubtedly confirms the feasibility of such strategy.

From the structure point of view, high-valent metals are quite different from low-valent ones. Their high charge over ionic radius makes the metal precursors highly reactive and oxophilic, tending to form large and rigid multi-nuclear secondary building blocks (SBUs) with high coordination number during MOFs formation, leading to structure diversity and enhanced framework ruggedness [58, 59]. For example, Zr(IV) ions in Zr-based MOFs could generate $Zr_6O_4(OH)_{12-n}(-COO)_n$ (n = 6, 8, 10 or 12) SBUs with different coordination numbers. Incorporating diverse Zr-based SBUs with various choices of polytopic organic ligands, such as dicarboxylic acid, tricarboxylic acid and planar tetracarboxylic acid, abundant MOFs architectures have been constructed, boosting the rapid growth of the field of Zr(VI)-based MOFs [60].

In this regard, Ti or titanium is considered a most appealing candidate for construction of MOFs with high chemical stability and structural diversity. Titanium is just above zirconium in the periodic table, thus also a typical tetravalent element in ionic form, while the much smaller ionic radius of $Ti^{4+}$ comparing to $Zr^{4+}$ grants it stronger affinity to oxygen. Actually,

$TiO_2$ is only soluble in highly acidic media (pH $\leq$0). Such stability could also be inherited by Ti-based MOFs constructed from Ti-oxo-carboxylate SBUs with strong Ti-O bonds. The most fascinating feature of Ti is, however, its well-known multifunctionality, typically, redox activity (transition between $Ti^{3+}$ and $Ti^{4+}$), photochemical property, and biocompatibility [61]. Possibility to engineer the optical band gap and integrate additional functional moieties by modification of organic ligands and nano-engineering has also attracted intensive interests from the traditional $TiO_2$ community [62-65]. Efforts to construct Ti-based MOFs could date back to the early days of MOFs, mostly failed, resulting in a wide range of amorphous and nonporous coordination polymers and compounds [66, 67]. These researches instead benefited the rich field of Ti-cluster chemistry. The discovery of first crystalline and porous carboxylate-based Ti-MOF, MIL-125, was as late at 2009 by Serre and coworkers [68]. Only since then the field has slowly yet considerably grown. New concepts and technics from other MOF-related researches like post-synthetic methods and covalent-combination method were introduced to overcome the difficulties encountered in direct solvothermal method, and the use of Ti-clusters instead of highly active Ti-alkoxides as Ti source greatly expanded the potential structure designability as well as improved crystallinity of products. Up to date there are only less than 20 Ti-based MOFs reported, including those derived from other MOFs structures by methods like post-synthetic metal exchange. However, the potential of these few MOFs has already drawn vast attention, and several hundreds of works have been published in wide fields. Except for some general applications of MOFs like gas storage and separation, Ti-MOFs have shown their unique potential, especially in photocatalytic redox reaction, pollutant degradation, water splitting, sensors and so on [69, 70].

Recently, Assi *et al*. exhaustively concluded in their insightful review paper the development of Ti-based coordination compounds during the past three decades, especially the richness of Ti-clusters and the efforts to construct Ti-MOFs [69]. The paper is quite instructive in understanding the chemistry of Ti-MOFs, but there is no discussion in this article or other review papers focusing on the wide and rapidly growing application of Ti-MOFs, specifically their unique photochemical properties. In this review, we will concentrate on the recent significant research progresses of Ti-MOFs, especially their

photocatalytic applications and corresponding mechanism. Unique topological structures and synthetic strategies of Ti-MOFs will also be discussed, as well as the major challenges in current research and outlooks for future works.

## 2. Synthesis of Ti-MOFs

Synthesis of Ti-based MOFs is undoubtedly one of the most challenging topics in MOFs field. Up to date, reported MOFs based on titanium are still rather scarce comparing to other metals, many of them only discovered recently. Such situation is probably due to the special chemistry of Ti cations and corresponding Ti compounds used as Ti source in MOFs synthesis. Ti(IV) is the stable state under ambient condition, while Ti(III) could also exist under reductive conditions but quickly oxidized back to Ti(IV) upon exposure to oxygen. Due to the low electronegativity and strong polarizing ability, $Ti^{4+}$ is highly reactive and strongly hydrolyze even under ambient humidity. Such high reactivity during MOFs synthesis generally causes fast and uncontrollable nucleation and irregular framework growth, eventually lead to formation of amorphous coordination polymer or mixture of various phases and clusters. Control over the reactivity of Ti precursors is the key factor in Ti-MOFs synthesis, which concerns careful selection of solution combination, concentration, temperature and time, and, if necessary, addition of modulators and auxiliary technologies like microwave and ultrasonication, and most importantly, choice of Ti source. The synthetic methods of several reported Ti-MOFs are listed in Table 1 and will be discussed in this review.

**(Insert Table 1 herein)**

### 2.1. Titanium precursor

Titanium precursors used in MOFs synthesis include the following kinds: hydrous $TiO_2$, titanium chlorides, titanium alkoxides, titanium complexes and titanium-oxo-clusters. Hydrous $TiO_2$ was only used in limited early reports for the synthesis of some titanium organic phosphonates, like MIL-22 [71] and MIL-25 [72]. These compounds, though composed of highly ordered frameworks, have rather small organic fraction and no accessible porosity, resembling inorganic titanium phosphates more than MOFs. Notably, the first porous Ti-MOF in the modern sense, MIL-91, was first synthesized with hydrous $TiO_2$ and

N,N'-piperazinebismethylenephosphonic acid ($H_4L$, L=$O_3P$-$CH_2$-$NC_4H_8N$-$CH_2$-$PO_3$) under hydrothermal condition [73]. The limitation of hydrous $TiO_2$ including high reaction temperature (>200 °C), long reaction time (3-4 d) and highly corrosive and toxic reaction media (40 % HF aqueous solution), severely impeded its utilization in MOFs synthesis.

Titanium chlorides are barely used in Ti-MOFs synthesis due to their vigorous hydrolysis releasing hydrochloride acid vapor under ambient condition [74]. One exception is $TiCl_3$, which is used in direct synthesis or post-synthetic metal exchange to construct the Ti(III)-analogue of some conventional di- or trivalent MOFs, in which case Ti(IV) species could not be utilized due to unbalanced charge and mismatched ionic radius. The highly reductive nature of $Ti^{3+}$ requires delicate operation during experiments, and exposure to air would definitely lead to failure of synthesis. Typically, Mason *et al.* successfully synthesized a Ti(III) analogue of MIL-101 from $TiCl_3$ and terephthalic acid by solvothermal method under $N_2$ protection [75].

The most commonly used Ti source in MOFs synthesis so far is titanium alkoxides, or $Ti(OR)_4$ (R is an alkyl group). Introduction of hydrophobic alkoxy groups together with steric hindrance suppresses the hydrolysis of $Ti^{4+}$, and reactivity could be tuned to some extend by changing the alkoxy chain. From Table 1 it is clear that the most widely used $Ti(OR)_4$ in MOFs synthesis is titanium tetraisopropoxide ($Ti(iOPr)_4$) considering its commercial abundance and good solubility in most organic solvents. It should be noted that in $Ti(OR)_4$, the coordination number of Ti (4) is lower than its stable state in $TiO_2$ (6), so these compounds are still highly unstable and reactive. The uncontrolled reaction of these compounds in many cases lead to the failure of efforts to grow large single crystals, and structures of products have to be resolved based on powder X-ray diffraction (mostly, from synchrotron beams), adding additional difficulties to the task.

Utilization of stable six-coordinated Ti compounds or pre-formed well-defined Ti-oxo-clusters with a general formula $Ti_nO_m(OH)_x(COOR)_y$ is an exploitable way to control the reaction degree during MOFs formation [67, 76, 77]. Thanks to the richness of Ti cluster

chemistry, a variety of Ti-clusters with different sizes, geometry and coordination numbers could be selected as potential building blocks of MOFs. However, there is no guarantee that the original cluster could be preserved in the final MOFs structure. For example, in the synthesis of PCN-22, the highly-symmetric $Ti_6O_6(iOPr)_6(abz)_6$ (abz = 4-aminobenzoate or $H_2N$-$C_6H_4$-COO) was used as Ti source, but the $Ti_6$-oxo cluster was totally transformed during reaction into an unprecedented $Ti_7O_6$-oxo SBU in the final MOFs [77]. In another case, the same hexameric Ti cluster was preserved as SBU in the formation of MOF-901 [78] and MOF-902 [79]. Consequently, the Ti clusters serve either as building blocks to directly construct MOFs, or simply as relatively stable Ti preservers that continuously release Ti ions during reaction. In either case, the use of Ti clusters instead of Ti alkoxides is beneficial to tune the reaction rates and acquire larger single crystals. Though related reports are rather limited now, the use of Ti-clusters as precursors should be considered a potential future trend for designable and controllable synthesis of Ti-MOFs.

**2.2. Direct synthesis**

Direct synthesis by conventional hydrothermal/solvothermal methods is still the most commonly used method for synthesis of Ti-MOFs. Organic ligands and titanium precursors were dissolved (or dispersed) in suitable solvents and loaded into a Teflon-lined steel autoclave or sealed Pyrex vial, and heated under autogenous pressure with reaction time from several hours to days. Solvents play an important part in the crystallinity of final products, and often best combination of solvents has to be found by trail-and-error. Concentration of reactants is another key factor determining the morphology of produced MOFs. In one example, amine functionalized MIL-125 ($NH_2$-MIL-125) microcrystals, could be tuned from circular plate to octahedron by simply changing the concentration of starting solution [80].

In the early stage, hydrothermal reactions were employed for the construction of a series of titanophosphates [71-73] and oxalatotitanates [81] (unfortunately, most of them were nonporous), including the first porous Ti-MOF, MIL-91 [73]. In 2009, the well-known prototypical Ti-MOF, MIL-125, also the first crystalline and porous carboxylate Ti-MOF, was achieved under solvothermal reaction by Serre and coworkers [68]. Reaction of $Ti(iOPr)_4$ and

the organic ligand, terephthalic acid, in an appropriate proportion of solvent mixtures (N,N'-dimethylformamide (DMF) and methanol) at 423 K for 15 hours successfully led to well crystallized white powder of MIL-125. The amine functionalized analogy of MIL-125, namely $NH_2$-MIL-125, was also prepared by replacing terephthalic acid with 2-aminoterephthalic acid, in a similar solvothermal reaction process [82].

A series of Ti-salicylate MOFs were also successfully synthesized by solvothermal methods from $Ti(iOPr)_4$ and 2,5-dihydroxyterephthalic acid ($H_4$DOBDC). In 2014, high quality, robust, red and hexagonal prism single crystals of a Ti-MOF, NTU-9, were synthesized by Zhang and coworkers *via* conventional solvothermal reaction of $Ti(iOPr)_4$ with $H_4$DOBDC in acetic acid, which were stable in air, water and common organic solvents [83]. In 2016, Devic and coworkers systematically investigated homologous NTU-9 system by changing experimental parameters, and four Ti-MOFs named as NTU-9-like, MIL-167, MIL-168 and MIL-169 were successfully synthesized thorough solvothermal reactions between $H_4$DOBDC ligand and Ti precursors [76].

By using conventional solvothermal reaction at 180 ºC for 4h, the first three-dimensional (3D) extended Ti catecholate MOF (Ti-CAT-5) was successfully synthesized *via* combining the Ti ion and hexatopic catecholate linker, 2,3,6,7,9,11-hexahydroxytriphenylene ($H_6$THO) by Yaghi *et al.* in 2015 [84]. Meanwhile, dark red, plate-like crystals of a porphyrin-based Ti-MOF, PCN-22, was prepared by Zhou and coworkers under solvothermal reaction of $Ti_6O_6(OiPr)_6(abz)_6$ as the metal source, tetrakis(4-carboxyphenyl) porphyrin (TCPP) as the organic linker, and benzoic acid as a modulating reagent through solvothermal condition at 423K in N,N'-diethylformamide (DEF) solvent [77]. In the same year, by employing a hydrolytically more robust organometallic Ti precursor, dicyclopentadienyl titanium(IV) dichloride ($[Cp_2Ti^{IV}Cl_2]$), De Vos and coworkers presented a Ti-MOF, COK-69, built up from solvothermal reaction of $[Cp_2Ti^{IV}Cl_2]$ with *trans*-1,4-cyclohexanedicarboxylic acid ($H_2$cdc) in DMF in the presence of acetic acid as a synthesis modulator at 110 ºC for 48h under Ar atmosphere and subsequent air oxidation [85]. Utilizing solvothermal reaction between terephthalic acid and $TiCl_3$ in anhydrous DMF and ethanol at 120 °C under $N_2$ pressure with

stirring for 18 h, a titanium(III) analogue of MIL-101, namely Ti-MIL-101, was obtained by Long and coworkers [75].

In addition to Ti compounds as the only inorganic components in Ti-MOFs, some heterometallic Ti-MOFs have also been synthesized *via* the conventional solvothermal reaction. After the solvothermal reaction of a DMF solution containing $Zn(NO_3)_2 \cdot 6H_2O$, $Ti(OiPr)_4$ and 2-hydroxyterephthalic acid in a glass vial, block-shape orange crystals of a zinc-titanium-organic framework, ZTOF-1, was synthesized by Chun and coworkers [86]. When a mixture of zinc(II) nitrate and $Ti(iOPr)_4$ reacted with 3-hydroxy-2,7-naphthalenedicarboxylic acid ($H_3$ondc) and 1,4-diazabicyclo-[2.2.2]octane (dabco) in DMF under solvothermal reaction, orange-colored, hexagonal, column-shaped crystals of a zinc-titanium-organic framework, ZTOF-2, were also achieved by the same group [87]. Thus, conventional hydrothermal/solvothermal method is still commonly used for the preparation of Ti-MOFs.

Beyond conventional solvothermal methods, some auxiliary technologies, such as microwave [88, 89] or ultrasonic [90], have also been introduced into direct synthesis of porous Ti-MOFs. Assistant of such technics could benefit the crystallization process, shortening reaction time and lowering reaction temperature. Moreover, Ti-MOFs synthesized by such alternative routes often possess different particle sizes and morphologies that can affect their properties. By considering the rapid heating characteristic of microwave procedure, attempts were firstly made to prepare $NH_2$-MIL-125 *via* a solvothermal method [88]. Reaction time was shortened from 16h for conventional solvothermal method to 1h under microwave heating. The acquired powders were identified by powder X-ray diffraction (PXRD) to be phase-pure, while the average particle size (0.7μm) was smaller than that of solvothermal one, since particle growth was limited by shorter reaction time, and the rapid heating promoted nucleation. For the case of ultrasonication, the formation and collapse of bubbles formed in the solution produce very high local temperature and pressure, and thus result in extremely fast heating and cooling rates, which offer a good condition for producing fine crystallites. The intense shear forces can lead to the formation of excited molecules,

accelerating the dissolution of the starting materials and bond breakage-formation process. Han and coworkers have reported that $NH_2$-MIL-125 synthesized *via* ultrasonic-aided solvothermal method exhibited a uniform size distribution of around 300 nm [90]. Using microwave/ultrasonic/solvothermal combined method, a continuous and defect-free Ti-MOFs membrane on porous $TiO_2$ disc was also successfully fabricated [91].

### 2.3. Coordination-covalent combination method

Though most of the reported Ti-MOFs were constructed by direct synthesis, such approach has shown serious limitation concerning the special nature of Ti-coordination chemistry. The complex Ti-O condensation during MOFs synthesis frequently lead to formation of unpredicted structures and byproducts, and among numerous attempts to construct Ti-MOFs, most ended up with the discovery of some new Ti-coordination clusters. As discussed above, use of Ti-oxo-clusters as titanium source can to some extend decrease such uncertainty by directing MOFs construction around preformed clusters into pre-designed topologies. However, for direct synthesis, from discrete clusters to connected SBUs, the monotopic ligands in the original clusters have to be exchanged by the corresponding polydentate ligands without changing their geometry and nuclearity, which is not the case in most situations. The clusters either totally dissolved (e.g. MIL-169) or partially disassembled and reorganized into some new SBUs (e.g. PCN-22), in neither way the original purpose of using clusters was achieved.

To think conversely, if the Ti-O bonding within clusters were not disturbed during reaction, the original cluster structure and coordination mode could be readily preserved as SBUs in the final MOFs. Inspired by the construction of covalent-organic frameworks (COFs) [92, 93], a new strategy was proposed combining the synthesis of metal- and covalent-organic frameworks. Here we name it the coordination-covalent combination strategy considering the bonding nature of both MOFs and COFs. Yaghi and coworkers group presented the first successful example of such strategy [78]. A structure-known discrete Ti cluster with amine functionalized carboxyl ligands, $Ti_6O_6(iOPr)_6(abz)_6$, was used as Ti source. Utilizing the imine condensation reactions of the -$NH_2$ group on abz ligand with benzene-1,4-dialdehyde

(BDA), which is a representative bonding pattern in COFs construction, they attempted to build Ti-MOFs with known topology and structure. Limited by the low solubility of the obtained cluster in a variety of solvents, only poorly crystallized powders or amorphous solids were obtained in the stepwise synthesis process. The *in-situ* covalent combination in the presence of BDA gave the final formation of a robust Ti-MOF, MOF-901. Subsequently, when changing the organic extender from BDA to 4,4'-biphenyldicarboxaldehyde (BPDA), MOF-902 that contains longer aldehyde linking unit was also obtained utilizing the same method [79]. An important point of this work is that all the reactions were completed in one-pot, saving the steps to separately synthesize and separate metal clusters. Formation of coordination and covalent bonds could proceed simultaneously without interrupting each other, allowing the *in-situ* generation of Ti-clusters together with framework assembly. This report is also among the very few reports of such strategy across the whole MOF field [94], probably due to the stability of Ti-based clusters over other metal-organic polyhedrons (MOPs) [95, 96]. Nevertheless, the potential of such strategy is yet to be exploited. The various combinations of Ti-clusters and covalent extenders might promote the fast development of the Ti-MOFs field, especially considering the rich connectivity and functionality that could be integrated on the organic extenders.

### 2.4. Post-synthetic cation exchange method

Ti-MOFs fabricated by direct synthesis are often structurally unpredicted. Post-synthetic cation exchange is thus considered a useful method for preparation of Ti-MOFs with targeted pore and/or topology structures starting from structure-known MOFs constructed from other metal ions [97, 98]. This approach could also avoid the high reactivity and vigorous hydrolysis of Ti precursors. Exchanging with $Zr^{4+}$ of the same group and valence gives the most straightforward examples of such approach. The prototype Zr-MOF, UiO-66, was taken as the first example for post Ti-exchange by Cohen *et al*. [99]. After post-synthetic cation exchange, it was verified that >90 % of the microcrystalline MOFs particles contain Ti(IV), with about 38 wt% Ti(IV) content in the sample. Moreover, no change took place in the crystallinity of Ti-exchanged UiO-66(Zr/Ti) (Figure 1). Hill and coworkers reported that smaller pores in Ti-exchanged UiO-66(Zr) can enhance the $CO_2$ isosteric heat, and

consequently increase $CO_2$ uptake (enhanced by 81 %) [100]. By introducing diamine-substituted ligands into the Ti-cation exchanged UiO-66, the resulted sample greatly enhanced the photocatalytic ability for $CO_2$ reduction under visible light irradiation [101]. Ti-exchanged UiO-66 can also drastically enhance gas transport performance in membranes [102]. Moreover, bimetallic Zr(Ti)-NDC-MOF (NDC = 2,6-naphthalen-di-carboxylate) was prepared by the incorporation of Ti(IV) into Zr(IV)-NDC-MOF [103]. The effect of Ti on their Lewis acid catalytic properties was evaluated, and the results revealed that the Zr(Ti)-NDC-MOF showed higher activity and selectivity than the parent Zr-NDC material. The validity of such process was proven by many groups, yet some basic scientific issues are still not solved, like the exact coordination environment of Ti within the exchanged frameworks. As well-known, Zr in UiO-66 or its analogs is eight-fold coordinated, but Ti generally presents a six-fold octahedral coordination mode in most of its MOFs and coordination compounds. Insertion of Ti into the Zr-based SBUs inevitably leads to unmatched coordination, with formation of either Ti ions with higher coordination number, or defects and local deformation, but currently there is no solid experimental evidence like EXAFS results for either case.

**(Insert Figure 1 herein)**

As compared to tetravalent ions, most MOFs are constructed from di- or trivalent metal ions, and the unmatched charge and ionic radius hinder the direct exchange of high valent $Ti^{4+}$ with these metal species. A high valence metathesis and oxidation (HVMO) strategy is thus developed by Zhou *et al*. [104], starting from $Ti^{3+}$ which is more compatible with low-valent metal ions, followed by oxidation of exchanged Ti(III) centers into Ti(IV) by exposure to air. Such method can be considered as the further development of original post-synthetic metathesis (PSM) method [105]. In the process of this strategy, stable trivalent MOFs (MIL-100(Sc) and PCN-333(Sc)) and divalent MOFs (MOF-74(Mg) and MOF-74(Zn)) were selected as starting templates, and by utilizing the HVMO method, a series of porous photoactive Ti-MOFs, including Ti-PCN-333, Ti-MIL-100, and Ti-MOF-74, were successfully synthesized (Figure 2) [104]. The crystallinity of all fabricated Ti-MOFs were well maintained during the HVMO process, and all the prepared Ti(IV)-MOFs exhibited high

chemical stability and excellent photocatalytic activities. There are four factors affecting the success of this strategy: i) the metal cations in the original MOFs cannot be reduced by Ti(III); ii) the open metal sites should be contained, which could effectively accelerate the metathesis rate; iii) the coordination environment of the metal cations in the original MOFs should be similar to that of Ti(III), i.e. octahedral six-fold coordination; iv) metal-ligand bonds in original MOFs should be labile for driving the metal ion exchange. Overall, the Ti-cation exchange method provides a novel route to synthesize new functional Ti-MOFs with known structures.

**(Insert Figure 2 herein)**

### 2.5. Vapor-assisted crystallization method

Although Ti-MOFs have shown high potential as heterogeneous catalysts, the intrinsically microporous structures limit their applications. One of the solution is creating mesopores in MOFs structures, which is however hard to control in traditional solvothermal reactions. Hicks *et al.* introduced a vapor-assisted crystallization method (VAC), and a hierarchically microporous/mesoporous MIL-125 exhibiting interparticle mesoporosity was synthesized through the use of a surfactant cetyltrimethylammonium bromide (CTAB) [106]. In the structure of prepared materials, two kinds of pores were formed. The micropores were resulted from the dissolution of the embedded matrix in a solvent during a solvothermal process, while the capping agent CTAB controlled particle growth and helped the formation of mesopores between MOFs nanoparticles. The resulted hierarchical MOFs showed excellent catalytic oxidation of dibenzothiophene with tertbutyl hydroperoxide due to the presence of large amounts of unsaturated metal sites.

### 2.6. Synthesis of Ti-MOF composites

It is well known that MOFs supported metal nanoparticles have been widely used as effective catalysts, and efforts have also been made to prepare highly dispersed nanoparticle-doped Ti-MOFs. Noble metal nanoparticles, such as silver (Ag) [107, 108], gold (Au) [90], platinum (Pt) [109], and palladium (Pd) [110-112], as well as non-noble metal nanoparticles, such as nickle (Ni) [113] have been successfully imbedded into the pores of

Ti-MOFs. For instance, Pd nanoparticles were imbedded into the $NH_2$-MIL-125 *via* photo-assisted deposition method by Yamashita *et al.* in 2013 [111], which displayed higher catalytic activity at ambient temperature on account of photoactive Ti ions from the Ti-MOFs support. Meanwhile, graphene-like $MoS_2$ sheets, $Ag_2S$, CdS, and CuS quantum dots were also deposited onto MIL-125, and a series of Ti-MOFs based composites were formed under UV light conditions. These composites were utilized as photocatalysts for Cr(VI) reduction under visible light irradiation [114].

Owing to their unique photochemical properties derived from Ti-based moieties, efforts have also been devoted to fabricating other Ti-MOF based composites. For example, graphitic carbon nitride, reduced graphene oxide (rGO) or graphene, and titanium dioxide ($TiO_2$) were complexed with $NH_2$-MIL-125 to generate Ti-based materials including $C_3N_4$/$NH_2$-MIL-125 [115], rGO/$NH_2$-MIL-125[116], $NH_2$-MIL-125/$TiO_2$ [117, 118], and CuO/MIL-125 [119], proving effective in achieving enhanced optical, photoelectric, electrochemical, and photocatalytic properties.

## 3. Structure of Ti-MOFs

Although the construction of Ti-MOFs has been intensively investigated, reports of intrinsic Ti-based structures with 3D connected frameworks and accessible porosity are still relatively limited. Even among the reported few examples, Ti-MOFs have exhibited their intriguing highly unpredictable and variable structural nature with unprecedented SBUs and topologies unseen in other MOFs. It seems that, based on experience from limited successful cases and reference from Ti-cluster chemistry, ligands have a strong directing effect towards the finally formed Ti-oxo SBUs, hence the structures of Ti-MOFs will be discussed in detail based on different kinds of ligands, including phosphonates, carboxylates, salicylates and catecholates. It is noteworthy that currently all the reported Ti-MOFs are based on Ti-O bonds, and coordination of Ti with other atoms in MOFs is yet to be explored.

### 3.1. Phosphonate based Ti-MOFs

Early research of Ti-MOFs was the extension of inorganic Ti-phosphonates [120]. Férey *et al.* reported a series of titanophosphate based Ti-MOFs, typically MIL-22 [71], MIL-$25_n$ (n = 2, 3) [72], and MIL-91(Ti) [73]. MIL-22 and MIL-$25_n$ (n = 2, 3) were prepared with diphosphonic acid, $H_2O_3P$-$(CH_2)_n$-$PO_3H_2$ (n = 1 for MIL-22 and 2, 3 for MIL-$25_n$). The monoclinic MIL-22 is constructed by corner-shared trimers of Ti-oxo octahedrals and $PO_4$ from diphosphonic linkers, forming 2D array of microporous channels. The triclinic MIL-$25_n$ with expanded linkers show 3D Ti-oxo pillared structures linked by soft alkyl chains. These compounds, though having 3D connected framework structures, do not have accessible pores to nitrogen even after guest removal. The first porous Ti-MOF is MIL-91, firstly reported by Serre *et al.* in 2006 [73]. The monoclinic framework of MIL-91 is constructed from corner-sharing chains of $TiO_6$ octahedral linked by $HPO_3C$ groups from $H_4L$ linkers, with a significant Brunauer-Emmett-Teller (BET) surface area of 500 $m^2/g$. MIL-91 showed high hydrothermal stability and potential application of $CO_2$ capture because of its ultra-high $CO_2/N_2$ selectivity [121], but the harsh reaction condition limited its further research.

### 3.2. Carboxylate based Ti-MOFs

In the limited Ti-MOF structures, most Ti-MOFs with known frameworks are constructed from carboxylate ligands. When reacting with polydentate carboxylate acids, Ti cations tend to form large Ti-oxo-carboxylate clusters of high nuclearity and coordination number, resulting in the highly variable structures of as-formed Ti-MOFs. The formation of the Ti-oxo-carboxylate clusters originates from the partial hydrolysis and following polycondensation of Ti precursors, where water comes from the esterification between unreacted carboxylate acids with alcohols either *in-situ* formed from reacted Ti-alkoxides or purposely introduced into solvents. The multinuclear clusters are consisted of edge and/or corner sharing $TiO_6$ octahedra and linked together by carboxylate linkers.

#### 3.2.1. MIL-125 and $NH_2$-MIL-125

The first porous crystalline carboxylate-based Ti-MOF is MIL-125, first reported in 2009 by Férey *et al*, by direct solvothermal synthesis [68]. White fine powders of MIL-125 were acquired and structure was resolved based on synchrotron powder XRD. The framework of

MIL-125 (Figure 3) is consisted of cyclic $Ti_8O_8(OH)_4(COO)_{12}$ octamers with edge- and corner-sharing $TiO_5(OH)$ octahedra, linked by terephthalic linkers. The SBUs arrange in a centered cubic (cc) manner, packing into the quasi-cubic tetragonal lattice, and each octamer has 12 SBU neighbors. The 3D framework provides two types of cages corresponding to the octahedral and tetrahedral vacancies of cc packing, with effective accessible diameters of 12.55 Å and 6.13 Å, respectively, and connected through triangular windows of 5-7 Å. MIL-125 is thermal robust (stable up to 360 °C) and highly porous with a BET surface area and pore volume of 1550 $m^2/g$ and 0.65 $cm^3/g$, respectively. The amino-functionalized analog, $NH_2$-MIL-125, was successfully synthesized latter, with corresponding BET surface area of 1130 $m^2/g$ [82]. As compared with MIL-125, $NH_2$-MIL-125 is more stable against moisture because of the intramolecular hydrogen bonding between the aromatic amino hydrogen atoms and carboxylate oxygen atoms in the structure. Moreover, Yot and coworkers investigated the structural behaviors of MIL-125 and $NH_2$-MIL-125 under mechanical stimuli by high-pressure PXRD up to 3.5 GPa [122]. The solids showed a gradual pressure-induced reversible decrease of their crystallinity. Modifications of the phenyl rings of MIL-125 with other functional groups were also reported. Discovery of MIL-125 triggered the research of Ti-MOF in a real manner, paving the ways for both discovery of new Ti-MOF structures and development of various applications.

**(Insert Figure 3 herein)**

### 3.2.2. COK-69

A new Ti-MOF based on the combination of *trans*-1,4-cyclo- hexanedicarboxylate (cdc) linkers and an unprecedented $[Ti^{IV}_3\text{-}(\mu_3\text{-}O)(O)_2(COO)_6]$ cluster was recently reported by Bueken *et al*., namely COK-69 [85]. Blue-gray microcrystalline solid of reduced COK-69($Ti^{III}$) was obtained under nitrogen protected solvothermal condition, which was rapidly transformed into off-white solid, COK-69 ($[Ti^{IV}_3\text{-}(\mu_3\text{-}O)(O)_2(cdc)\cdot DMF]_n$), in air. In COK-69, three neighboring Ti atoms jointed by a $\mu_3\text{-}O^{2-}$ ion and six carboxylates give the formation of the $Ti_3O_3$ cluster. The cluster is then connected by six $cdc^{2-}$ linkers to form the porous framework of COK-69 featuring both trigonal-bipyramidal cages and one-dimensional hexagonal channels with an *acs* topology as that of the well-known MIL-88 family. Due to

the conformational flexibility of the $cdc^{2-}$ linker, structural changes, also called as breathing effect, from the closed-pore (2.7Å, with a low $S_{BET}$ = 29 $m^2/g$ after activation) to the open-pore (4.9Å) takes place by the immersion of COK-69 in low-polar solvents, such as DMF and methanol (Figure 4).

**(Insert Figure 4 herein)**

### 3.2.3. PCN-22

The first porphyrin-based Ti-MOF, PCN-22, was synthesized from reaction between the preformed $Ti_6O_6(OiPr)_6(abz)_6$ clusters and tetrakis(4-carboxyphenyl)-porphyrin (TCPP) ligands under solvothermal condition [77]. Infrequently, dark red, plate-like single crystals were successfully obtained and resolved. In the structure of PCN-22, the original hexameric Ti-cluster are completely reorganized into an unprecedented $Ti_7O_6$ oxo-cluster, which can be regarded as two $Ti_3O_3$ trimers linked by a bridging Ti atom. Each $Ti_3O_3$ trimer, similar to that in COK-69, is connected to six TCPP ligands forming a 2D layer. Assembly of these layers *via* inserted Ti atoms results in the 3D framework of PCN-22 with tetragonal channels of *ca.* 1.5nm. Topologically, each $Ti_3O_3$ can be regarded as a 6-connected node and a TCPP linker can be seen as a 4-connected node, and then, the overall structure can be simplified into a novel (4,6) connected net with a point symbol of (Figure 5).

**(Insert Figure 5 herein)**

### 3.2.4. MOF-901, MOF-902

MOF-901 was acquired by one-pot synthesis as described above [78]. Its hexameric $Ti_6O_6(OCH_3)_6(abz)_6$ cluster is well determined during the stepwise synthetic process, which is a trigonal prismatic $Ti_6O_6$ inner core surrounded by six equatorial, planar, and chelating terminal abz ligands. The planar SBUs are linked together, forming a perforated 2D layer with triangular apertures (14 Å in width). The 2D layers stacked with an interlayer distance of *ca.* 3.47 Å in a AB manner, forming 1D channels on the vertical direction. MOF-901 exhibits permanent porosity with a BET surface area of 550 $m^2/g$. MOF-902, isoreticular to MOF-901, was synthesized through the same synthetic process, only by replacing the reactant BDA by

longer organic ligand BPDA [79]. The expanded MOF-902 showed larger triangular windows of *ca.* 16 Å but a lower BET surface of 400 $m^2/g$ (Figure 6).

**(Insert Figure 6 herein)**

### 3.2.5. Ti-MIL-101

Ti-based analogy of a highly porous MOF, Ti-MIL-101, the first all-titanium(III) metal organic framework with permanent porosity, was also fabricated by using Ti(III) chloride as the metal source and terephthalic acid as the organic linker [75]. Structure analysis towards the dark-purple powder of Ti-MIL-101 revealed that it has a face-centered-cubic unit cell with $a$ = 89.78(2) Å. The Langmuir and BET surface area of the activated Ti-MIL-101 were 4440 and 2970 $m^2/g$, respectively, with a total pore volume of 1.50 $cm^3/g$. Five-coordinated Ti(III) centers of Ti-MIL-101 could react with $O_2$ to form titanium(IV) superoxo and peroxo species. More importantly, such a distorted trigonal-bipyramidal coordination geometry can effectively inhibits strong adsorption of nonredox-active gases because of shielding Ti(III) charge after desolvation.

## 3.3. Salicylate based Ti-MOFs

The successful synthesis of Ti-MOF-74 and its expanded absorption into the visible-light region together with enhanced photoactivity demonstrates a useful strategy of using organic linkers with salicylate moieties including neighboring phenolic hydroxyl and carboxylate groups such as $H_4$DOBDC for band-gap engineering of Ti-MOFs. The phenolate-Ti bond is known to induce ligand-to-metal charge transfer (LMCT), thus deepening the apparent color of the solid and enhancing light absorption within the visible region [76, 123]. The phenolate O presents stronger basicity than carboxylate oxygen, thus stronger bonding with the Lewis acidic Ti center. Also, the neighboring position of phenolate and carboxylate groups on the benzene ring enables the formation of stable hexatomic rings when both coordinated with the same Ti center. In this sense, introduction of salicylate moieties on ligands could also improve the chemical stability of Ti-MOFs. The neighboring phenolate O could compensate one of the coordination sites on the $TiO_6$ octahedron, saving an oxo or hydroxyl oxygen, thus significantly decreases the degree of Ti-O polycondensation and the nuclearity of as-formed

SBUs. Actually, in the few reported Ti-salicylate MOFs, most show a single-nuclear $Ti(O_{phenolate})_3(O_{carboxylate})_3$ SBU from the coordination of a Ti center with three salicylate ligands.

### 3.3.1. ZTOF-1 and ZTOF-2

The first example of Ti-salicylate MOF is a heterometallic Zn/Ti-MOF, ZTOF-1, reported by Hong *et al.* in 2013 [86]. A simple asymmetrical dicarboxylate ligand, 2-hydroxyterephthalic acid ($H_3$obdc) was reacted together with zinc and titanium precursors under solvothermal condition to give the orange crystals of ZTOF-1. Structure analysis revealed that ZTOF-1 possesses a double-walled primitive cubic net. In ZTOF-1, Ti coordinates with the "salicylate" end of the ligand while Zn coordinates with the carboxylate end, and a $Zn_6Ti_2$ cluster with an internal center of inversion symmetry is *in-situ* generated, which can be considered as formate bridged $Zn_3Ti$ unit formed by titanium capping of the $Zn_3(\mu_3\text{-}OH)(CO_2)_6$ moiety. The $Zn_6Ti_2$ heterometallic clusters are then extended by 12 obdc ligands along six mutually perpendicular directions to give the formation of porous ZTOF-1 with one-dimensional straight open channels ($3 \times 4.5$ Å$^2$) dispersedly filled by dimethylammonium cations. Later another heterometallic Zn/Ti-MOF in a formula of $[H_2N(CH_3)_2][Zn_3(\mu_3\text{-}OH)Ti\text{-}(obpdc)_3(O_2CH)]$ was synthesized by extending the organic linker from $H_3$obdc to 2-hydroxy-4,4'-biphenyldicarboxylic acid ($H_3$obpdc) [124]. This structure is isoreticular to ZTOF-1 and also possesses the double-walled primitive cubic net (pcu).

ZTOF-2 was synthesized by replacing $H_3$obdc by longer asymmetrical dicarboxylate ligand, $H_3$ondc with the addition of dabco in the synthetic process, and orange hexagonal column-shaped crystals were obtained [87]. Analysis of ZTOF-2 revealed two distinct clusters in the crystal. One is sandwich shaped cluster with a $[Zn_3(\mu_3\text{-}CO_3)(OH_2)_3]$ center capped by two tris-chelated Ti(IV) moieties, giving a final nodal geometry of a trigonal prism. The other is a trinuclear Zn-cluster, $[Zn_3(CO_2)_6(dabco)]$, in a pinwheel geometry. The connection of two kinds of clusters finally forms the overall (6,8)-connected net of ZTOF-2, which can also be described as the trapezo-rhombic dodecahedron with an imaginary sphere of 16 Å diameter

and two types of windows having 4-7 Å diameter. Though the two ZTOF show totally distinct topologies, they share the same $Zn_3Ti$ cluster and coordination mode of Ti with the salicylate part of asymmetric ligands. Both MOFs show high permanent porosity towards various gases and high BET surface area of 1045 $m^2/g$ for ZTOF-1 and 1878 $m^2/g$ for ZTOF-2 (Figure 7).

**(Insert Figure 7 herein)**

### 3.3.2. NTU-9

The first pure Ti-salicylate MOF was reported in 2014 by Zhang and coworkers by solvothermal reaction of $Ti(OiPr)_4$ with $H_4$DOBDC in acetic acid, resulting in red hexagonal prism crystals of NTU-9 [83]. NTU-9 crystallizes in the trigonal system with space group of *P*-31*c*. Instead of Ti-cluster, each Ti atom in NTU-9 is octahedrally coordinated by six oxygen atoms, half from hydroxide groups and half from carboxylate groups, i.e. from three salicylate groups from DOBDC, giving the formation of 2D honeycomb-like layers, the parallel stacking of which forms 1D channels with about 11 × 11 Å along the *c* axis. After removing guest molecules in the channels, the solvent-accessible void in the structure of NTU-9 was calculated to be about 50.7 % by PLATON program, but its permanent porosity was not accessed by experiments (Figure 8).

**(Insert Figure 8 herein)**

### 3.3.3. NTU-9-like, MIL-167, MIL-168 and MIL-169

Reaction between Ti and $H_4$DOBDC under different conditions gave a series of structures with different topologies aside from NTU-9 [76]. Solvothermal reaction carried out in DEF instead of acetic acid gave a solid with the formula of $Ti(H_xDOBDC)_{1.5}(DEAH)_y \cdot n(DEF)$ (DEAH = diethylammonium) and 2D layered structure very similar to that of NTU-9, namely NTU-9-like. Addition of methanol in the starting solvent resulted in the formation of MIL-167, $Ti(DOBDC)_{1.5}(DEAH)_2 \cdot nH_2O$, constructed also from isolated $TiO_6$ octahedra linked by DOBDC linkers. The final solid was consisted of two interpenetrated enantiomeric 3D chiral networks of (10,3)-a topology, with free cavities of *ca.* 6-7Å in diameter. Adding catecholate (cat) as modulator to the DEF solution led to MIL-168, $Ti(DOBDC)(cat)(DEAH)_2$, where the $TiO_6$ octahedral was built up from two DOBDC ligands and one cat modulator,

forming 1D zigzag chains running parallel to each other and separated by N−H···O hydrogen-bonded DEAH cations.

MIL-169 was synthesized in a different system. A preformed tetrameric titanium oxalate cluster, $TiO_{0.5}(DOBDC)(H_2O)(pipH_2)_{0.5}\cdot H_2O$ ($pipH_2$ = piperazinium), was reacted with $H_4$DOBDC under hydrothermal condition to give the powders of MIL-169. Specially, MIL-169 is the only Ti-salicylate MOF reported to be consisted of condensed $Ti_2O_{11}$ dimers rather than isolated Ti octahedra. The dimers of octahedra bridged by a $\mu_2$-oxo group and terminal water molecules are connected by DOBDC ligands to afford anionic layers, and then further interacted with $pipH_2$ ions and free water molecules by hydrogen bonds.

### 3.4. Catecholate based Ti-MOFs

**Ti-CAT-5:** Catecholate based MOFs have shown highly promising applications in various fields recently. However, despite the richness of Ti-catecholate clusters, up to now only one Ti-MOF based on polycatecholate ligand was reported, which is Ti-CAT-5 [84]. Ti-CAT-5 was built up from isolated Ti-centers connected by the tritopic catechol derivative ligand, $H_6$THO, forming a highly extended anionic 3D framework. The ideal large aperture of this MOF was occupied by an identical framework, forming a double-interpenetrated structure with BET surface area of 450 $m^2/g$. Iron and vanadium analogs of Ti-CAT-5 were also isolated.

## 4. Photocatalytic application of Ti-MOFs

In the past several decades, titanium dioxide ($TiO_2$) has been considered as one of the most successful photocatalysts [61]. Although $TiO_2$-based photocatalysts including doped $TiO_2$ and $TiO_2$-based hybrids have been developed to reduce absorption energy below 3 eV and to separate photogenerated electrons and holes, it is still difficult to harvest photons within the visible light range, with other issues of low solar energy conversion efficiency, easy agglomeration, and difficult recyclability limiting their large-scale applications [125-127]. By introducing Ti ions into MOFs, some limitations such as agglomeration could be logically overcome. Distinct from other MOFs, Ti-MOFs have Ti species as essential inorganic

components in the frameworks, showing intriguing optical response or photoactivity. The high porosity and unique photo-responsive property of Ti-MOFs derived from their structure features make them highly promising porous materials in photo-related utilizations, including photocatalytic oxidation reaction, photocatalytic $H_2$ generation, photocatalytic organic pollutant degradation, photocatalytic $CO_2$ reduction, and photocatalytic sensors.

The first Ti-MOF showing attractive photochemical responses is the monumental MIL-125, together with its amino-analog, $NH_2$-MIL-125. As the first carboxylate-based Ti-MOF, discovery of MIL-125 is no doubt the trigger of the currently blooming Ti-MOF research field, stimulating both the development of new Ti-MOF structures and applications in various fields. A fast photochromic effect was discovered when the MOF was initially reported [68]. When adsorbed with alcohols in the cavities, MIL-125 presented a color change from white to dark blue under UV radiation without loss of crystallinity, and the process could be totally reversed by simple exposure to air. UV spectrum exhibited a new broad and intense band in the range of 400-800 nm, which should be related to the intervalence electron transfer resulted from optically induced hopping of electrons from Ti(III) to Ti(IV) sites in the titanium oxo-clusters of MIL-125. $NH_2$-MIL-125 also showed similar reversible photochromism [128]. The phenomenon was attributed to the light-induced partial reduction of $Ti^{4+}$ to $Ti^{3+}$ accompanied with oxidation of alcohols to aldehydes, clearly demonstrating the photo-redox properties of Ti-MOFs and their promising potential as photocatalysts for various applications.

### 4.1. Basic strategy

Two basic parameters to evaluate the performance of a photocatalyst include activity and efficiency. Activity is the most important property of a catalyst, generally expressed by turn-over frequency (TOF) or turn-over number (TON), corresponding to the number of reactant molecules converted by a single active site in unit time or given reaction time. Such parameters can most straightforwardly represent the intrinsic activity of catalysts. However, for complicate systems like Ti-MOFs and their composites, determination of actual active sites and their numbers is quite difficult, if not impossible, especially when catalysis is the result of synergism between different kinds of sites. Gravimetric specific activity based on the

total mass of catalyst is thus a widely accepted alternative in this case, especially from realistic point of view, where inactive components like supports are also counted in the mass of catalysts. Efficiency includes two aspects: the percentage of photons consumed by photocatalytic reaction in total absorbed photons, and the ratio of light absorbed by catalysts to the whole sunlight spectrum [129]. For the first one, most of the energy from absorbed photons is wasted by recombination of photogenerated electron-hole pairs and intermolecular energy transfer between dye molecules, thus a crucial point is to facilitate the separation of charge carriers. For the latter one, enhancing the light absorbance within the Vis-IR region, especially lowering the bandgap, is a key point for Ti-MOF based photocatalysts.

### 4.1.1. Bandgap engineering

Bandgap is an essential parameter of photocatalysts, which represents the lowest energy needed for an absorbed photon to generate an electron-hole charge carrier pair, which could further transport to active centers and drive the redox reactions. Though first reported with photocatalytic ability, the performance of MIL-125 was far from ideal. MIL-125, with an optical bandgap of *ca.* 3.6 eV ($\lambda$ = 345nm), was photoactive only under UV radiation [68]. Considering most of sunlight's energy and photons distribute within the visible-near infrared (Vis-NIR) region, it is much necessary to drive the photoactivity into the visible region, which requires bandgap engineering of the materials. Creating chromophores with visible and infrared absorption on the ligand is one option. The first example was $NH_2$-MIL-125, where introduction of the amino group onto the terephthalic acid ligand created another absorption band in the visible light region up to 550 nm, lowering the bandgap to 2.6 eV, and the MOF presented significant photoactivity towards $CO_2$ reduction under visible light radiation [128]. Inspired by this work, Hendon *et al.* combined experimental and computational methods to in-depth study the effect of ligand functionalization to optical bandgap [130]. By introducing a diaminated ligand, the bandgap was further lowered comparing to the single aminated $NH_2$-MIL-125, and a mixed-amine MIL-125 with 10% bdc-$(NH_2)_2$ and 90% bdc-$NH_2$ ligands was successfully synthesized with an experimental bandgap of 1.3 eV ($\lambda$ = 950 nm), remarkably shifting to the red/IR region. Post-modification, especially for the amino group of $NH_2$-MIL-125, is another commonly used approach to modulate the light absorbing ability of

the MOF system. Nasalevich *et al.* successfully introduced a dye-like moiety onto the amino groups of $NH_2$-MIL-125 by post-synthetic modification, greatly improved the absorption ability within the visible light region, expanding the cutoff wavelength to *ca.* 700 nm [131]. Introduction of functional groups may also bring additional benefits for photochemical properties besides lowering the bandgap. van der Veen and coworkers found that organic linker defines the excited-state decay of MIL-125-type Ti-MOFs [132]. They found that the amino group as the hole stabilizer in MIL-125 could prolong the lifetime of the photoexcited state as compared to that of MIL-125. Furthermore, Garcia *et al.* confirmed the photoinduced charge separation in $NH_2$-MIL-125 by using methyl viologen as the electron acceptor and N,N,N,N-tetramethyl-p-phenylene-diamine as the electron donor [133].

Functionalization of MIL-125 analogs has exhibited inspiring results, yet the potential of such approach is limited. Despite that it is not likely easy to further lower the bandgap below 1.3 eV, the rather big $Ti_8$-oxo clusters in MIL-125 structure much assemble inorganic Ti-O compounds, forming local semiconductive regions. These clusters are where active catalytic sites locate in most cases, but could be hardly affected by modification of ligands. Besides, blindly expanding absorption band may not effectively improve photocatalytic activity of MOFs as expected, for photons with too low energy not enough to drive photoreaction may also be absorbed. Another factor is steric hindrance induced by the introduction of additional groups on ligands, which partially block the apertures of MOFs and impede mass transport during catalytic reactions.

In this regard, except for modification of ligands, construction of new topologies and structures is an essentially important approach to engineer the bandgap of Ti-MOFs, yet a definitely more challenge one. Evidently, new porous Ti-MOFs only appeared years after the discovery of MIL-125. These new structures have shown intriguing intrinsic light absorbing properties (Figure 9). Expanding the aromatic conjunction system on ligands significantly lowered the bandgap of MOFs, which was, for example, lowered to 2.65 eV in MOF-901 [78] and 2.50 eV in MOF-902 [79]. PCN-22 with a porphyrin-based ligand shows a bandgap of 1.93 eV [77], lowest for pure carboxylate-based Ti-MOFs to date. Salicylate-based Ti-MOFs

present further improved light absorption, due to the strong LMCT effect between phenolate oxygen and Ti ions benefiting the transportation of photo-induced charge carries. The relative small Ti-SBUs may also be crucial in this context. MOF-74(Ti) has a low bandgap of 1.88 eV [104], and this number is even lower for NTU-9 (1.72 eV) [83]. Other salicylate-based Ti-MOFs also showed improved light absorption within the visible region, though exact bandgaps, either experimental or computational, were not reported. Considering the stronger LMCT, pure catecholate-based Ti-MOFs should present even stronger light absorption ability and lower bandgap. Unfortunately, the light absorption property of Ti-CAT-5 was not evaluated in published works, and no other catecholate-based Ti-MOF structures are yet reported to date.

**(Insert Figure 9 herein)**

### 4.1.2. Encapsulation of active species

Improving the reactivity of active sites presents another alternative strategy to improve the performance of photocatalysts by increasing the total photochemical efficiency. Noble-metal nanoparticles like Pt or Ru are the most widely utilized multifunctional catalysts with high performance towards many important reactions. Back to 1977, G. N. Schrauzer and T. D. Guth reported the first case of $Fe/TiO_2$ as photocatalyst towards $H_2O$ decomposition [134], leading to the establishment of the so-call photochemical mechanism [135]. In the case of MOF, encapsulation of Pt, Pd, Au or Ru nanoparticles within the pores of Ti-MOFs were also reported and applied to drive photocatalytic reactions [136, 137]. In such systems, the photo-generated electron-hole pairs are effectively separated, where electrons move to the surface of noble metal nanoparticles instead of Ti-containing SBUs and induce reduction reaction. The catalytic activity of coordination unsaturated Pt or Ru atoms is prominently higher than the intrinsic $Ti^{3+}$ sites in Ti-MOFs, in this way the overall photocatalytic activity is improved. Aside from noble metals, other functional species like $MoS_2$, heteropoly acids, quantum dots and carbon nanospecies could also be incorporated with Ti-MOFs, which requires further exploration.

## 4.2. Photocatalytic oxidation reaction

Ti-MOFs and Ti-MOF based composites have been employed as photocatalysts for photocatalytic oxidation of alcohols, aromatic alcohols, alkylphenols, hydrazine and so on. As aforementioned, the well-known robust Ti-MOF, MIL-125, showed a photoactive property upon UV-Vis excitation, where the photocatalytic reduction of Ti(IV) into Ti(III) was accompanied with the oxidation of alcohols, and meanwhile photocatalytic oxidation of Ti(III) into Ti(IV) can be associated with the reduction of $O_2$ into superoxide diatomic $[O_2]^-$.

Li *et al.* studied photocatalytic activity of $NH_2$-MIL-125 for the aerobic selective oxidation of amines to imines using $O_2$ under visible light irradiation (Figure 10) [138]. The results showed that benzylamine could be converted to N-benzylidene benzylamine using $NH_2$-MIL-125 photocatalyst under visible light irradiation, and the conversion and selectivity in $CH_3CN$ after 12 h irradiation were 73 % and 86 %, respectively. After the photocatalytic reaction for three runs, the crystal structure of $NH_2$-MIL-125 was not destroyed, and its photocatalytic activity remained unchanged, suggesting its structural stability and reusability. As compared with benzylamine, amines with electron donating substituents on the phenyl ring showed enhanced conversion (75-92 %) and improved selectivity (90-93 %). Photocatalytic aerobic oxidation of amines to imines over $NH_2$-MIL-125 revealed that the electron transferring from the excited ligand ATA to the Ti-O oxo-clusters led to the formation of $Ti^{3+}$ center. The highly active $Ti^{3+}$ further reacted with $O_2$ to form $\bullet O_2^-$ and was oxidized back to $Ti^{4+}$. In the meantime, photogenerated carbon centered radicals interacted with $\bullet O_2^-$ to form aldehydes. The nucleophilic attack on aldehydes by amines thus produced corresponding imines *via* the dehydration.

**(Insert Figure 10 herein)**

Ti-MOF based composites, such as noble-metal (Au, Pd or Pt) nanoparticle doped MIL-125, can also improve conversion and selectivity of photocatalytic oxidation reaction, reported by Wu *et al*. [109]. M/MIL-125 (M = Au, Pd, Pt) composites were synthesized by a facile $Ti^{3+}$-assisted method, where an in situ redox reaction between reductive $Ti^{3+}$-MIL-125 and oxidative metal salt precursors occurred without using extra reducing or stabilizing agents. The average diameters of Au, Pd, and Pt nanoparticles immobilized into the cavities of

MIL-125 were about 6, 3, and 3 nm, respectively. Importantly, the doping of Au, Pd, or Pt nanoparticles did not destroy the crystal structure of MIL-125, and no characteristic peak of Au, Pd, or Pt nanoparticles was observed due to low loading and even distribution of the nanoparticles. The high photocatalytic performance of M/MIL-125 can attribute to a Schottky barrier between MIL-125 and noble metals, allowing photoelectrons to easily transfer from MIL-125 to noble metal nanoparticles because of their interfacial contact. In photocatalytic selective oxidation of benzyl alcohol reaction, the conversions using Au@MIL-125, Pd@MIL-125 and Pt@MIL-125 under reactions for 4 h at 298K were 36.0 %, 32.7 % and 26.4 % respectively, significantly higher than that of MIL-125 (18.9 %).

The photocatalytic properties of Ni-doped $NH_2$-MIL-125 in the selective aerobic oxidation of aromatic alcohols to their corresponding aldehydes using $O_2$ as the oxidant were studied by Zhu and coworkers [113]. As compared with $NH_2$-MIL-125, Ni-doped $NH_2$-MIL-125 showed a significant improvement in the photocatalytic activity, i.e., the conversions of p-methyl benzyl alcohol using $NH_2$-MIL-125 and Ni-doped $NH_2$-MIL-125 were 25.8 % and 43.2 %, respectively. It was also confirmed that Ni nanoparticles encapsulated inside the pores of $NH_2$-MIL-125 had a mean diameter of 3 nm. The enhanced photocatalytic activity of Ni-doped $NH_2$-MIL-125 should be resulted from the visible-light harvesting and photo-induced charge transfer by doping of Ni nanoparticles into $NH_2$-MIL-125. Moreover, $N_2$ adsorption/desorption, powder XRD characterizations and three-cycle experiments revealed that the structure and photocatalytic activity of used Ni-doped $NH_2$-MIL-125 after the 3rd-run reaction were almost identical to the fresh one, further confirming the stability of Ni-doped $NH_2$-MIL-125.

Long *et al*. reported a sandwich-like hierarchical nanoarchitecture composed of reduced graphene oxide (rGO) and photoactive MOF materials. Photocatalytic oxidation of 4-nitrobenzyl alcohol, 4-methylbenzyl alcohol, and 4-fluorobenzyl alcohol were chosen to explore the photocatalytic mechanism of sandwich-like hybrids under visible light irradiation at ambient temperature [116]. It was shown that the addition of rGO improved the photocatalytic performance of MOFs no matter what groups on the phenyl ring. Due to

supreme carrier mobility of graphene, photogenerated charge carriers could transfer and separate more efficiently. Therefore, upon visible light irradiation, photogenerated electrons quickly transfer onto the graphene layer, and $O_2$ absorbed on graphene is then reduced to $[O_2]^-$ species. Meanwhile, aromatic alcohols are oxidized to positive radical carbonium ions by deprotonation. Finally, positive radical carbonium ions react with $[O_2]^-$ species to produce corresponding aromatic aldehydes. However, excessive rGO would shield the MOFs from absorbing visible light and reduce the concentration of photogenerated charges, consequently prohibiting photocatalytic reactions.

### 4.3. Photocatalytic $CO_2$ reduction

An attractive strategy for decreasing greenhouse gas ($CO_2$) in air is to develop a novel material for reduction of $CO_2$ under visible light irradiation. Photoactive Ti-MOFs become ideal candidates for such propose. The photocatalytic reduction of $CO_2$ to $HCOO^-$ in the presence of triethanolamine (TEOA) under visible light irradiation over $NH_2$-MIL-125 was firstly investigated by Li *et al.* [128]. The amino functionality was proved crucial for the photocatalytic activity of $NH_2$-MIL-125 under visible light. The LMCT band induced by the amino group strongly absorbed visible light, generating a long-lived excited charge separation state with an electron transferred to $Ti^{4+}$ in the Ti-oxo center, reducing it into $Ti^{3+}$. The $Ti^{3+}$ sites thus worked as active centers to reduce $CO_2$ whereas TEOA served as both sacrificial electron donor and Lewis base. Subsequently, Li *et al.* investigated the photocatalytic performance of $CO_2$ reduction over different noble metal/$NH_2$-MIL-125 (Pt- and Au-) under visible-light irradiation in saturated $CO_2$ [136]. Noble metal nanoparticles in the cavities of $NH_2$-MIL-125 as electron traps can provide redox reaction sites and lower overpotential. Over 8 h irradiation, Pt/$NH_2$-MIL-125 had a positive effect on photocatalytic reduction (about 21 % increase, 12.96 μmol), while Au/$NH_2$-MIL-125 showed a negative activity for this reaction (about 16 % decrease, 9.06 μmol) as compared to photocatalytic activity for formate formation using pure $NH_2$-MIL-125 (10.75 μmol). The possible reason is that stronger Pt-O bond (391.6 $KJ \cdot mol^{-1}$) enables the supported Pt nanoparticles to bind with the adjacent oxygen to produce a stable structure, while the Au atom prefers the bridging site between two neighboring N atoms of $NH_2$ because of weaker Au-O bond (221.8 $KJ \cdot mol^{-1}$). Therefore, the

spillover of hydrogen from noble metal to the bridging oxygen linked Ti atoms for promoting the formation of $Ti^{3+}$ can be achieved over Pt/$NH_2$-MIL-125 instead of Au/$NH_2$-MIL-125.

Lee *et al.* reported highly efficient and robust Ti(IV) cation exchanged UiO-66-derivative (1(Zr/Ti)) incorporating $NH_2$-bdc and $(NH_2)_2$-bdc mixed ligands as an effective photocatalyst for $CO_2$ reduction to HCOOH under visible light irradiation with the aid of 1-benzyl-1,4-dihydronicotinamide and TEOA (Figure 11) [101]. As compared with UiO-66(Zr/Ti)-$NH_2$ (4.66 ± 0.17), 1(Zr/Ti) gave higher turnover number (6.27±0.23) of the Ti site towards $CO_2$, indicating that more electrons were accepted by Ti than Zr to catalyze $CO_2$. Two conduction band minimum values of the constructed 1(Zr/Ti) were calculated to be -0.84 eV and -2.10 eV, suitable for the $CO_2$ reduction. Additionally, the introduction of $(NH_2)_2$-bdc ligands greatly enhanced the photocatalytic ability by generating new energy levels for additional light absorption and charge transfer. The $^{13}C$ NMR spectrum indicated that the carbon source of HCOOH was $CO_2$, and the good stability and reusability of the catalysts were also confirmed.

**(Insert Figure 11 herein)**

### 4.4. Photocatalytic $H_2$ generation from water splitting

Studies have demonstrated that Ti-MOF photocatalysts can be used to promote photocatalytic hydrogen production from water splitting [139]. Matsuoka and coworkers investigated the hydrogen production from an aqueous medium over MIL-125, $NH_2$-MIL-125, Pt/MIL-125 and Pt/$NH_2$-MIL-125 under visible light irradiation at wavelengths up to 500 nm, where Pt was loaded into MOF by photodeposition method [137]. Among these solids, Pt/$NH_2$-MIL-125 was the most efficient visible-light-responsive photocatalyst without losing its photocatalytic activity during at least three cycles. The total production of $H_2$ reached 33 μmol over Pt/$NH_2$-MIL-125 after 9 h of irradiation. $NH_2$-MIL-125 exhibited slightly lower photocatalytic activity, while Pt/MIL-125 showed no photocatalytic activity under the same condition. Therefore, -$NH_2$ groups in organic ligands and Pt nanoparticles as co-catalysts both played an indispensable role on promoting the photocatalytic hydrogen production under visible-light irradiation. Wu and coworkers then studied the possibility of $H_2$ generation *via*

water splitting over M/MIL-125 composites (M = Au, Pd, or Pt) prepared from a new $Ti^{3+}$-mediated method [109]. The total production of $H_2$ over Pt/MIL-125 obtained through the $Ti^{3+}$-assisted method was 38.68 μmol under visible-light irradiation for 5 h. As compared with Pt/MIL-125-PD prepared by a direct photodeposition method, the turnover number of Pt/MIL-125 (30.2) was about 80 % higher, showing that encapsulation method has an essential effect on the catalytic properties of metal nanoparticle/Ti-MOF composites.

Non-noble metal cooperated Ti-MOF composites were also utilized for photocatalytic water splitting and $H_2$ generation. Nasalevich *et al.* reported an efficient and fully recyclable catalytic system, cobaloxime-derived Ti-MOF photocatalyst, for light-driven hydrogen evolution from water under visible-light illumination (Figure 12) [140]. The introduction of catalytically active Co sites led to a 20-fold enhancement of $H_2$ evolution activity to that of $NH_2$-MIL-125. More importantly, Co@$NH_2$-MIL-125 showed a high stability with a constant turnover frequency (0.8 $h^{-1}$) after 65 hours of irradiation, and without loss of activity after several recycling experiments. The catalytic potential of Co@$NH_2$-MIL-125 was lower than that of the LUMO of $NH_2$-MIL-125. The photogenerated hole at the organic linker reacts with the sacrificial electron donor, while the electron is rapidly injected into the cobalt species, leading to the reduction of Co(III) to Co(II). The presence of high-spin Co(II) species improves the photocatalytic activity of the whole system. The Ni/$NH_2$-MIL-125 composite containing a highly active proton-reducing nickel(II) catalyst [Ni(dmobpy)(2-mpy)$_2$] (dmobpy = 4,4'-dimethoxy-2,2'-bipyridine, and 2-mpy = 2-mercapto-pyridyl) was prepared and investigated as hydrogen evolving catalyst from water splitting by Meyer *et al*. [141]. It was shown that, in 5 v/v% TEOA aqueous conditions, the amount of produced hydrogen over Ni/$NH_2$-MIL-125 composite was two orders and one order of magnitude higher than that of $NH_2$-MIL-125 and Ni species, respectively. In 2 v/v% water and acetonitrile mixture, Ni/$NH_2$-MIL-125 showed the turnover frequency of 28 mol $H_2$ $g(Ni)^{-1}$ $h^{-1}$ with high stability and photocatalytic activity (sustaining catalysis for more than three times).

**(Insert Figure 12 herein)**

Recently, studies also showed that, using MIL-167 itself, a noticeable production of hydrogen was detected from water splitting only under UV irradiation ($\lambda$ = 280 nm) [76]. The

reason for no catalytic activity under visible illumination was not yet fully understood. Deeper investigations are still needed.

### 4.5. Photocatalytic organic pollutant degradation

MOFs have been studied as a new class of photocatalysts for potential applications in environmental fields, such as organic pollutant degradation [142-145]. *P*-type semiconductor NTU-9, a stable crystal in air, water and common organic solvents, displayed a broad range of absorption from 400 nm to 750 nm with a bandgap of 1.72 eV. As compared with the bandgap of $TiO_2$ (3.2 eV for anatase), MIL-125 (3.6 eV) and $NH_2$-MIL-125 (2.6 eV), the adsorption of NTU-9 showed obvious red shift. Under visible-light irradiation, NTU-9 exhibited remarkable photocatalytic activity and photostability in the degradation of rhodamine B (RhB) and methylene blue (MB) aqueous solution [83]. It was shown that RhB and MB were completely photodegraded after 80 min and 20 min under a 300 W Xenon lamp irradiation, respectively.

Some methods have been developed to prepare novel photocatalysts based on Ti-MOFs for organic pollutant degradation, which include post-synthetic modification and metal nanoparticle loading [107, 108]. For instance, Ag nanoparticle-decorated MIL-125 microspheres (Ag/MIL-125) were synthesized (Figure 13) [108], in which Ag nanoparticles were dispersed on the surface of MIL-125 microspheres with a uniform diameter of about 40nm. Ag acted as a co-catalyst, and the prepared Ag/MIL-125 exhibited excellent photocatalytic efficiency. Photogenerated $[O_2]^-$ and •OH from ambient oxygen and hydroxyl groups from aqueous solution serve as the main reactive species in the photodegradation of RhB. Under visible light irradiation, RhB was almost completely degraded in 40 min over Ag/MIL-125 with 3 wt% Ag NPs loading, and the photocatalytic degradation activity of the hybrid was four times higher than that of commercial P25. Moreover, the photocatalyst can be reused at least five times without obvious loss of its photocatalytic activity.

**(Insert Figure 13 herein)**

Abdelhameed *et al.* successfully improved photocatalytic activity and chemical stability of $NH_2$-MIL-125 by incorporating Cr(III) and Ag nanoparticles into the pristine MOF, in which

the amino groups were firstly treated with acetylacetone (AC) [107]. Under visible-light irradiation, MB was almost completely degraded in the presence of Cr-MIL-125-AC and Ag-MIL-125-AC, where Cr(III) acted as the hole acceptor and Ag nanoparticles as the electron acceptor, promoting the separation of electron-hole pairs and increasing the recombination time. The prepared Ag-MIL-125-AC was an efficient and chemically stable photocatalyst in MB degradation, the photodegradation rate constant of which remained the same value (0.10 $min^{-1}$) for five recycling reactions.

Yuan and coworkers reported the Ag/rGO/MIL-125 ternary hybrids, exhibiting more efficient photocatalytic performance for RhB degradation in water under visible light irradiation [146]. The apparent rate constant of Ag/rGO/MIL-125 for RhB degradation (0.0644 $min^{-1}$) was 1.62 times higher than that of pure MIL-125 (0.0396 $min^{-1}$). The photocatalytic activity of Ag/rGO/MIL-125 slightly decreased probably due to the loss of photocatalyst in recycling photocatalytic experiments, indicating the stability of Ag/rGO/MIL-125 for the RhB degradation. Due to efficient charge transport of rGO nanosheet, rGO acts as the electron transporter and collector, leading to excellent charge separation efficiency. Additionally, Ag nanoparticles could serve as efficient electron reservoir.

Different from metal-doped photocatalysts, other heterostructure Ti-MOF composites were also reported, such as g-$C_3N_4$/MIL-125 [115], core-shell $In_2S_3$/MIL-125 [147], and BiOBr/$NH_2$-MIL-125 [148], and used as efficient photocatalysts for the photodegradation of organic dyes, pesticides and antibiotics under visible light illumination. Importantly, these 2D layer materials (g-$C_3N_4$, $In_2S_3$, and BiOBr) as the supporter were found to have potential photocatalytic activity under visible light illumination. The enhanced photocatalytic performance under visible light illumination could often be attributed to the $Ti^{3+}$-$Ti^{4+}$ intervalence electron transfer and synergistic effect of components (such as π-π interactions, hydrogen bonding and electrostatic interactions), resulting in higher separation efficiency of photogenerated electron–hole pairs during the photocatalytic reaction. Furthermore, cake-like N-doped anatase/rutile mixed phase $TiO_2$ (A/R N-$TiO_2$) was successfully prepared via the

pyrolysis of MIL-125 and subsequent annealing at different temperature in ammonia atmosphere [149, 150]. The degradation rate of RhB for A/R N-$TiO_2$, obtained for the second annealing at 500 °C, increases to 93% in 240 min, which is higher than that of $TiO_2$ (32 %) under visible light irradiation. The increased light absorption and reduced electron-hole pair recombination enhanced photocatalytic performance of cake-like A/R N-$TiO_2$.

### 4.6. Photocatalytic polymerization

Isoreticular structural MOF-901 and MOF-902 exhibited high performance in photocatalytic polymerization of various monomers, such as methyl methacrylate (MMA), benzyl methacrylate (BMA), and styrene, under visible light in the presence of ethyl α-bromophenylacetate as a co-initiator [78]. The polymers with high molecular weight, high yield, uniform distribution and low polydispersity index were produced in organic solvents under visible light irradiation. For example, the molecular weight, yield and polydispersity index of the prepared polyMMA in the presence of MOF-901 catalyst loading of 0,034 mol% after 18 h reaction was 26850 g/mol, 87 % and 1.6, respectively. As compared with MOF-901 (*ca.* ~2.65 eV), MOF-902 absorbed the visible light in red-shifted region, leading to lower optical bandgap (*ca.* ~2.50 eV). Larger conjugated linker units in MOF-902 containing more electron donors could assist to stabilize free radicals during the reaction process, affording polymer chains with a bromide end group. Therefore, in polymerization reactions, MOF-902 exhibited better performance as a heterogeneous photocatalyst than MOF-901 and other MOFs possessing similar band-gap energy. Meanwhile, the crystal structure, surface area and photocatalytic activity of MOF-901 and MOF-902 remained unchanged after at least three consecutive cycles, suggesting their high chemical and reactive stability in organic solvents.

### 4.7. Photocatalytic deoximation reaction

A surfactant-assisted version of $NH_2$-MIL-125, SMIL-$NH_2$, was prepared *via* solvothermal method in the presence of Pluronic P123 as a structure-directing agent by Morsali *et al.* [151]. The photocatalytic property of SMIL-$NH_2$ was evaluated by deoximation reactions. In an energy efficient photocatalytic system, the nanostructured SMIL-$NH_2$ was able to catalyze the regeneration of carbonyl compounds from various oximes at the rate two times higher than

that of $NH_2$-MIL-125. When the yield of photocatalytic deoximation reaction of oximes in the presence of SMIL-$NH_2$ achieved 100 %, the reaction time of acetophenone oxime converting into the corresponding ketone was 10 h, while the reaction time of activated acetophenone oxime with electron-donating substituents such as methyl and methoxy units was shorten to 6 and 4.5 h, respectively. Furthermore, SMIL-$NH_2$ was significantly stable under the reaction conditions and could be easily recycled after the reaction, showing significant retention of its photocatalytic activity.

**4.8. Photocatalytic sensors**

Having unique optical response and photophysical properties, Ti-MOFs have also been utilized as photoelectrochemical sensors as other MOFs [152, 153]. Long-term stability is one of the most important properties of sensors. Hu and coworkers studied photooxidation assisted sensitive detection of trace $Mn^{2+}$ in tea by $NH_2$-MIL-125 modified carbon paste electrode ($NH_2$-MIL-125/CPE) [154]. $NH_2$-MIL-125/CPE showed an efficient photooxidation activity toward $Mn^{2+}$ in $NH_3$-$NH_4Cl$ (0.04 M) buffer (pH = 8.5) under visible light. Stripping peak currents on $NH_2$-MIL-125/CPE had a good linear relationship with the concentration of $Mn^{2+}$ in the range from $1.0 \times 10^{-8}$ to $1.0 \times 10^{-5}$ M with the detection limit of $4.0 \times 10^{-9}$ M. Importantly, the sensitivity of $NH_2$-MIL-125/CPE on monitoring $Mn^{2+}$ remained nearly unchanged after 100 repeated uses, indicating its stability. Meanwhile, the electrode retained 96.5% response and 3.12% relative standard deviation (RSD) for monitoring $1.0 \times 10^{-6}$ M of $Mn^{2+}$ after 30 days' storage at room temperature, and can also be polished to expose a fresh layer for reuse, suggesting its storage stability.

A sensitive photoelectrochemical sensor for the determination of the herbicide clethodim was also reported by Hu *et al.* [117], which was constructed by using $NH_2$-MIL-125/$TiO_2$ modified glassy carbon electrode as working electrode. Upon visible light irradiation, the photoexcited electrons were delivered to the glassy carbon electrode, while the photogenerated holes reacted with $H_2O$ to generate hydroxy radicals (•OH). The generated •OH was attacked by clethodim, leading to an enhanced photocurrent. Under the optimal experimental conditions, clethodim could be quantified in the concentration range from 0.2 to

25 μmol/L, with a detection limit (3 S/N) of 10 nmol/L. More importantly, $NH_2$-MIL-125/$TiO_2$/GCE sensor retained 94.1 % of its original response after 7-day storage at 4 °C in humid environment, showing its high storage stability.

A europium (Eu) functionalized $NH_2$-MIL-125, MIL-125-AM-Eu, as a turn-off fluorescence sensor for detection of α-phenethyl alcohol, was developed by Yan *et al.* (Figure 14) [155]. Upon UV light irradiation, the fluorescence signal that was originated from the $^5D_0 \rightarrow {}^7F_2$ 4f electron transition of $Eu^{3+}$ firmly attached to MIL-125-AM could be observed, and its intensity became weaker upon time until fluorescence was fully quenched (about 20 min). When α-phenethyl alcohol was adsorbed into the channels of MIL-125-AM-Eu, the photoactive Ti(IV) could promote the oxidation of α-phenethyl alcohol, informing corresponding acetophenone. Carbonyl groups produced by the oxidation hence caused the fluorescence attenuation. Moreover, powder XRD patterns of MIL-125-AM-Eu composite verified its structural stability after the recycling experiments. No distinct changes of luminescence emission intensity, photocatalytic conversion and Ti/Eu ratio after five cycles indicated its reusability for sensing α-phenethyl alcohol. The outstanding performance of the MIL-125-AM-Eu made it a turn-off fluorescence sensor for α-phenethyl alcohol. Meanwhile, they found that MIL-125-AM-Eu could also be utilized as ratiometric fluorescent sensor for anion recognition and detection.

**(Insert Figure 14 herein)**

## 5. Other applications of Ti-MOFs

### 5.1. Gas adsorption and separation

It is well known that hydrogen storage at 77 K strongly depends on structure properties of porous materials, such as surface area, microporous volume and pore shape [12]. Latroche and coworkers studied the influence of amino groups on hydrogen binding and adsorption capacity by comparing MIL-125 and $NH_2$-MIL-125 [82]. $H_2$ adsorption capacity of MIL-125 and $NH_2$-MIL-125 was 3.4 and 2.5 wt% at 77 K and 4 MPa, respectively. At low pressure, no significant increase in the heat of adsorption was observed due to the amine group functionalization (a similar enthalpy of adsorption was about ~ 6 kJ/mol), whereas at high

pressure, $NH_2$-MIL-125 showed lower $H_2$ adsorption capacity than that of MIL-125 because of decreased BET surface area.

Investigations have shown that the pore size of frameworks and the strength of interaction between $CO_2$ and MOFs played an important role on $CO_2$ adsorption and separation. Ahn *et al.* reported that the maximum $CO_2$ adsorption capacities were 176 and 96 mg/g for MIL-125, and 248 and 132 mg/g for $NH_2$-MIL-125 at 1bar and 273 K and 298 K, respectively (Figure 15). Although the introduction of amine groups into framework decreased the BET surface area, $NH_2$-MIL-125 showed better $CO_2$ adsorption capacity than that of MIL-125 over the whole investigated temperature range, and an excellent $CO_2$ adsorption selectivity over $N_2$ (> 27:1) at 298 K due to the strong interaction between -$NH_2$ group and $CO_2$ molecule [88]. Wang *et al.* also examined the effects of amine groups toward $CO_2$ adsorption and $CO_2/CH_4$ separation at high pressures up to 10 bars by employing MIL-125, $NH_2$-MIL-125, and their isostructural MIX-MIL-125 constructed from the assembly of binary linkers with Ti(IV) ions [156]. Thermal stability of MIX-MIL-125 was improved due to existence of binary linkers. It was shown that both $CO_2$ and $CH_4$ adsorption could be increased when introducing amine groups into frameworks, while the selectivity factor of $CO_2/CH_4$ reduced after amino functionalization. Regufe *et al.* studied the gas adsorption equilibrium of $NH_2$-MIL-125 at 303, 323, and 343 K and pressures up to 7 bar, and the affinity of different adsorbates to $NH_2$-MIL-125 particles presented an order of $CO_2$ > $CH_4$ > CO > $N_2$ > $H_2$ [157]. These studies are complementary to each other, beneficial to the syngas purification.

**(Insert Figure 15 herein)**

Weireld and coworkers studied the purification of acid gases, $CO_2$ and $H_2S$ from biogas and natural gas using $NH_2$-MIL-125 [158]. The MOF chosen as the adsorbent was stable up to 373 K under water vapor without the framework destruction upon several adsorption-desorption cycles. Through investigations using combinational techniques of adsorption, microcalorimetry, IR spectroscopy and modeling, it was verified that suitable $CO_2$ and $H_2S$ adsorption enthalpies of $NH_2$-MIL-125 made it easier to capture acid $CO_2$ and $H_2S$ gases. Moreover, the amino group could enhance the $CO_2/CH_4$ selectivity (~7) due to the

existence of interactions with $CO_2$ in $NH_2$-MIL-125. On account of the presence of amine groups and the absence of Lewis acid sites, higher adsorption value ($\Delta(\Delta H(H_2S)–\Delta H(CH_4))$ (~18 kJ/mol) for $NH_2$-MIL-125 than that of MIL-125 (~12 kJ/mol) over the pressure range led to higher $H_2S/CH_4$ selectivity (~70) on $NH_2$-MIL-125.

Mixed matrix membranes (MMMs) incorporated with MIL-125 and $NH_2$-MIL-125 were synthesized and employed for $CO_2/CH_4$ and $CO_2/N_2$ gas separation reported by two research teams led by Vankelecom [159] and Friebe [160], respectively. They found that, by comparing with the neat polymer matrix, the addition of the Ti-MOF powder enhances both the permeability and the selectivity of $CO_2$ molecules.

Lau and coworkers reported that the incorporation of titanium ions into UiO-66 could enhance the gravimetric $CO_2$ capture [100]. Specifically, the incorporation of titanium ions may shrink the pore size within the framework ideal for $CO_2$ adsorption, and enhance the $CO_2$ isosteric heat ($Q_{st}$) to increase the $CO_2$ uptake. Additionally, lower framework density of Ti-exchanged UiO-66 also increased the $CO_2$ uptake. Smith *et al.* studied the $CO_2/N_2$ separation performance of Ti-exchanged UiO-66 loaded MMMs [102]. It was shown that the Ti-exchanged UiO-66 MMMs with only 5 wt% loading could drastically enhance the $CO_2$ permeability as high as 153 % as compared with UiO-66 loaded MMMs. Importantly, the strong interaction between the exposed metal centers of MOFs and the polymer matrix had significant effects on the formation of interfacial free volume, providing a significant increase in the gas permeability. Therefore, incorporating metal ions into Ti-MOFs and loading them onto MMMs may open up practical applications in $CO_2$ capture, storage and separation.

The uptake capacities toward $H_2$ and $CO_2$ by two Zn(II)-Ti(IV) heterometallic MOFs, ZTOF-1 and ZTOF-2, were studied by Chun's group [86, 87], revealing moderate uptake capacities for $H_2$, $CO_2$, and $CH_4$. The gas uptake capacities by ZTOF-1 at 1 bar were 150 $cm^3/g$ for $H_2$ at 77 K and 80 $cm^3/g$ for $CO_2$ at 273 K. The isosteric heat ($Q_{st}$) of $CO_2$ adsorption was 22 kJ/mol, which was comparable to other MOFs, such as UiO-66 (26 kJ/mol) and MIL-125 (21 kJ/mol). The uptake capacities of ZTOF-2 for $H_2$ (77 K), $CH_4$ (195 K) and

$CO_2$ (273 K) at 1 bar pressure were 1.74, 10.4, and 12.0 wt%, respectively. Therefore, the high density of open metal sites in these Ti-MOFs is believed to be advantageous for the gas storage.

### 5.2. Liquid phase adsorption and separation

In addition to gas phase adsorption and separation, the adsorption and separation properties of Ti-MOFs were also investigated in liquid phase. A column was packed by Rodrigues and coworkers using MIL-125 powder, and they subsequently studied the separation capability toward xylene isomers and ethylbenzene in liquid chromatography using *n*-heptane as the eluent at 313 K at low (≤ 0.8 M) and high (≥ 0.8 M) concentrations [161]. Results revealed that MIL-125, as a *para*-selective material, could separate *p*-xylene from other xylene isomers at low concentrations. A separation factor of 1.3 for *p*-xylene over *o*-xylene and *m*-xylene was obtained, while selectivity values of 1.5 and 1.6 for *p*-xylene over *m*-xylene and *o*-xylene were observed in a diluted ternary mixture, respectively. Meanwhile, Denayer *et al.* reported that MIL-125 packed column displayed a *trans*-selectivity for *cis*/*trans* difunctionalized cyclohexane molecules (1,3-dimethylcyclohexane and 4-ethylcyclohexanol) with high selectivity and resolution in liquid chromatograph [162]. Therefore, MIL-125 offers a perspective for stereoselective separations as the stationary phase in the application of liquid chromatograph.

On account of low volatility of chloroaromatic compounds, Ahn *et al.* studied the adsorption behavior of chloroaromatic compounds over MIL-125, $NH_2$-MIL-125, UiO-66, MIL-101, and $Cu_3(BTC)_2$ in the liquid phase. $NH_2$-MIL-125 and MIL-101 showed the effective adsorption of 2-chloroanisole in a mixture of equal amounts of chlorobenzene, 2-chlorotoluene, 1,3-dichlorobenzene and 2-chloroanisole in 1,3,5-triisopropylbenzene [163]. It was confirmed that high surface area and uniform microporosity of Ti-MOFs affected the adsorption capacity of 2-chloroanisole.

### 5.3. Electrode materials

In addition to the usage as photocatalysts and sensors as well as adsorbents, the application of Ti-MOFs in optoelectronics was also investigated as other MOFs. Recently, a new zinc-polyiodide redox flow battery (RFB) system with nanoporous $NH_2$-MIL-125 uniformly deposited onto the surfaces of graphite felts (GFs) was reported by Li and coworkers, demonstrating significantly enhanced energy density (Figure 16) [164]. The flow cells with $NH_2$-MIL-125 modified GFs serving as the positive electrode showed enhanced energy efficiency by about 6.4 % at the current density of 30 mA/cm$^2$ as compared to those achieved with pristine GFs. Therefore, the introduction of $NH_2$-MIL-125 with high-surface area to the GF surface can accelerate the $I^{3-}$-$I^-$ redox reaction, showing higher energy efficiency than that of pristine GFs. It was proven that long-term chemical stability of catalysts resulted from high coordination number between metal atom and oxygen can lead to stable cycling performance. The application of more MOFs in the field of RFBs will face new opportunities.

**(Insert Figure 16 herein)**

Ti-MOFs have been utilized for the fabrication of porous $TiO_2$ by pyrolysis. The resulting porous $TiO_2$ materials possessed high surface area, inter-connected hierarchical pores. When employed as anode materials for lithium ion batteries (LIBs) [165, 166], Na ion batteries (NIBs) [167] and solar cells [168], these MOF-derived porous $TiO_2$ exhibited superior rate capability, high reversible capacity and excellent long-term cycle stability. When tested as an anode material for LIBs, the as-prepared $TiO_2$ electrode presented a high reversible capacity of 122 mA·h/g after 1100 cycles at a high discharge/charge rate of 10C, and the Coulombic efficiency remained at nearly 100 % for each cycle [166]. Zhang *et al*. synthesized porous $TiO_2$/C composite through the calcination of MIL-125 under inert atmosphere [167]. When the as-prepared $TiO_2$/C composite was tested as anodes for NIBs, it exhibited superior cyclability with a reversible $Na^+$ storage capacity of 148 mA·h/g at the current density of 0.5 A/g after 500 cycles, and an outstanding rate performance with a capacity of 88.9 mA·h/g at the current density of 2.5 A/g. In another case, Kim *et al.* prepared shape- and morphology-controlled MIL-125 using poly(ethylene glycol)diglycidyl ether as a structure directing agent [168]. Solvothermal method followed by calcination afforded mesoporous hierarchical anatase $TiO_2$ (hier-$TiO_2$) with large surface area and high porosity. When

hier-$TiO_2$ was deposited onto a nanocrystalline $TiO_2$ (nc-$TiO_2$) layer as the scattering layer, the prepared hier-$TiO_2$/nc-$TiO_2$ bilayer photoanode based dye-sensitized solar cell (DSSC) exhibited greatly improved performance efficiency as high as 7.1 % at 100 mW/$cm^2$, as compared to the nc-$TiO_2$ monolayer photoanode based DSSC (4.6 %) or P25/nc-$TiO_2$ bilayer photoanode based DSSC (5.0%). Therefore, using the Ti-MOF template approach to prepare porous $TiO_2$ for electrode materials might pave a new way for developing high-performance porous $TiO_2$.

### 5.4 Heterogeneous catalytic reactions

MIL-125 and $NH_2$-MIL-125 showed superior selectivity to p-benzoquinones in the oxidation of alkyl-substituted phenols and 2,6-di-*tert*-butylphenol by using aqueous $H_2O_2$ as the oxidant and acetonitrile as the solvent [169]. Hierarchically microporous/mesoporous carbonaceous material supporting a high loading of Ti nanoparticles derived from the pyrolysis of MIL-125 revealed higher catalytic activity in the oxidation of the sulfur-containing dibenzothiophene than those of microporous materials, which should be attributed to the increased mesoporosity and smaller Ti nanoparticle sizes [170].

McNamara *et al.* investigated catalytic performance and stability of MIL-125 and MIL-47 (V-based MOF) in the oxidative desulfurization of heterocyclic aromatic sulfur compounds (dibenzothiophene, benzothiophene and thiophene) [171]. The reaction rate constants and conversion of MIL-47 outperformed MIL-125 in dibenzothiophene and benzothiophene oxidation experiments, while the catalytic activity of MIL-125 was higher than that of MIL-47 in thiophene oxidation experiment. Furthermore, MIL-125 also appeared stable in the presence of TBHP even under harsh reaction conditions. Through comparing catalytic activity of MIL-47 and MIL-125 in different catalytic oxidation experiments, it was suggested that an excellent catalyst should have the following properties: i) the reactants can be accessible to the active sites of catalysts in the pores, ii) the metal centers in MOFs appear to have higher activity sites in the catalytic oxidation reaction, and/or iii) catalytic reaction can take place both on the surface of the MOFs and inside the pores.

As an ideal support material for the immobilization of metal nanoparticles, Ti-MOFs have been employed increasingly as heterogeneous catalysts for some organic reactions. Pd nanoparticles have been deposited successfully on $NH_2$-MIL-125 and shown efficient and recyclable catalytic performance [110-112]. Yamashita *et al*. [110] found that Pd/$NH_2$-MIL-125 having Pd nanoparticles (9.2 nm) inside the pores of $NH_2$-MIL-125 rather than outside of the pores was the most active catalyst prepared *via* UV photo-assisted deposition method. The hydrolysis was nearly completed in 20 min with 250 μmol $H_2$ production, corresponding to 84 % of total $H_2$ content ($H_2$/AB = 3) (AB = ammonia borane). The TON of Pd/$NH_2$-MIL-125 with Pd loading of 0.25 wt% was 1051.1 $mol_{H_2}$ $mol_{cat}$. Meanwhile, they also found that the photo-assisted deposited Pd/$NH_2$-MIL-125 showed higher catalyst durability and catalytic performance on the dehydrogenation of formic acid at ambient temperature [111]. $H_2$ productions from Pd-TS-1, Pd−Ti-MCM-41, Pd-MIL-125 (photo-assisted), Pd-$NH_2$-MIL-125 (ion exchange) and Pd-$NH_2$-MIL-125 (photo-assisted) for 3 h were 1.7 μmol, 5.1μmol, 17.8μmol, 43.1μmol, 48.1μmol, respectively. Pd-$NH_2$-MIL-125 (photo-assisted) displayed the best catalytic performance, keeping almost its original activity after the recycling experiments. The TOF of the best-performing catalyst was 214 $h^{-1}$ for the Pd-$NH_2$-MIL-125 catalyst working at 305 K. As expected, -$NH_2$ groups in MOFs can prevent agglomeration of Pd nanoparticles on the framework, have a positive effect on the O−H bond dissociation, and contribute to higher catalytic performance at ambient temperature for formic acid decomposition. Indeed, weakly basic −$NH_2$ groups as proton scavenger form $-^{+}HNH_2$, while Pd-fomate species as reaction intermediate undergo β-hydride elimination to produce $CO_2$ and Pd hydride species.

Puthiaraj *et al.* found that Pd nanoparticle doped $NH_2$-MIL-125 exhibited excellent heterogeneous catalytic performance and reusability toward Suzuki cross coupling between aryl chlorides and arylboronic acids, while the reaction did not proceed in the presence of $NH_2$-MIL-125 [112]. It indicated the specific role of Pd nanoparticles as a catalyst in the Suzuki cross coupling reaction.

## 6. Conclusion and outlook

Titanium-based MOFs are no doubt one of the most fascinating yet challenging topics in the field of MOF research, especially considering their high thermal and chemical stability, novel structural diversity and photocatalytic properties. Regardless of decades of efforts resulting in the rich Ti-cluster coordination chemistry, the breaking development of Ti-MOF field only happened within the recent few years, with the discovery of MIL-125 as the milestone. Ti-MOF structures discovered up till now are still rather scarce comparing to other di-, trivalent and Zr-based MOFs, majorly due to the high volatility and hydrophilicity of ionic Ti precursors. In this review, we discuss the basic aspects of Ti-MOF chemistry such as synthetic strategy and structures, then focus on the photocatalytic applications by Ti-MOFs and their composites, including photocatalytic oxidation, $CO_2$ reduction, hydrogen evolution, organic pollutant degradation, polymerization, deoximation and photocatalytic sensors. For wider interest of readers, we also briefly introduce the application of Ti-MOFs in other fields like gas and liquid phase adsorption and separation, catalytic reaction, and electrochemistry.

Ti-MOFs have shown intriguing structural diversity unseen in other MOFs. Even the reported intrinsic Ti-MOF structures are less than 20, several of them have shown unique framework topologies, assembled from unprecedented SBUs and various organic ligands (organodiphosphonates, carboxylates, salicylates and catecholates). Ti precursors undergo spontaneous hydrolysis with water either residue in solvents, purposely introduced, or *in-situ* generated from reaction, usually forming relatively large multinuclear Ti-oxo-clusters as SBUs (*e.g.* the octamer in MIL-125), as well as amorphous $TiO_2$ which partially blocks the pores of as-formed MOFs. Increasing the complexing ability of ligands leads to smaller Ti-oxo clusters or even isolated Ti octahedra (*e.g.* in NTU-9), as well as suppresses the side reaction of competitive $TiO_2$ formation. Considering that only limited systems were reported, mostly from common organic ligands, there is still a lot of space to explore for new Ti-based MOF structures. It is noteworthy that all the reported Ti-MOFs are based on Ti-oxygen coordination bonds, and nitrogen or sulfur based ligands are scarcely investigated. To the best of our knowledge, only one example of N-based Ti coordination polymer with 2D networks was reported hitherto [172]. Due to the strong oxophilic nature of Ti cation, construction of

such structures could be very difficult in presence of any oxygenated source (solvent, Ti precursor, atmospheric oxygen, etc).

Synthesis is the major challenge in Ti-MOF research, majorly due to the highly unpredicted polycondensation of $Ti^{4+}$ cation, resulting in uncontrolled products. Other synthetic parameters like solvent composition, reaction temperature and time, and addition of surfactants and modulators also have great effects on the structure, crystallinity, porosity and morphology of final products. Direct solvothermal synthesis is currently the most common method for the synthesis of Ti-MOFs, but control over the structure of products is largely empirical and especially hard (if not totally impossible) when investigating a new system. We thus propose three possible strategies feasible for development of new Ti-MOFs: i) high valence metathesis and oxidation method. Starting from structural-known MOFs, corresponding Ti-analogs could be achieved by post-synthesis metal exchange, and followed by oxidation by simply exposing to atmosphere if necessary. Though arguments still exist, for example in the Ti-exchanged Ti/Zr-UiO-66, the coordination environment of Ti is still unknown, while in the case of MOF-74, Dincă *et al.* proposed that cation exchange in the MOF-74 family might not be possible because distortion of the 1D SBUs chains would require a large activation energy [98], yet Zhou *et al.* reported the successful synthesis of Ti-exchanged Mg- and Zn-MOF-74 [104]. Regardless, cation exchange should still be considered a useful method to synthesize Ti-MOFs, especially considering that many of them could not be easily achieved by direct solvothermal synthesis. ii) isoreticular expansion. By replacing ligands with elongated ones, Ti-MOFs with known topology but expanded pores would possibly be acquired. Such strategy is especially useful for MOFs with 1D channeled structures (e.g. the MOF-74 series, or MOF-902 for Ti-MOF). In other cases, expanding ligands may rise other issues like changed topology or interpenetration. iii) covalent-coordination combined strategy. As successfully demonstrated by MOF-901 and MOF-902, it is possible in one-pot reaction to spontaneously assemble the SBUs by coordination bonds and frameworks by covalent bonds. Ti is particularly suitable for such approach because of the stability and richness of Ti-oxo-clusters. Utilizing such strategy together with other techniques, it might be possible to finally achieve target-oriented synthesis

of Ti-MOFs with pre-designed topology and chemical functionality, while a first step should be the successful assembly of a Ti-MOF with 3D interconnected rather than 2D layered structure.

Compared with pure Ti-MOFs, multi-component guest/Ti-MOF composites show great advantages in photocatalytic applications especially under visible light illumination. Generally, the presence of metal nanoparticles as co-catalysts, embedded into the caves of Ti-MOFs, plays an important role in enhancing photocatalytic activities. Coupling with guest materials with suitable band potential is feasible to lower the electron-hole recombination rate and improve the photocatalytic activity. A 2D layered structure semiconductor like $TiO_2$, g-$C_3N_4$, metal sulfides, and BiOBr as the supporter of Ti-MOFs would offer an efficient photon capture, charge separation, and electron transport due to their synergism effect. Especially, the rGO nanosheet can provide a high-speed charge transfer channel, leading to enhanced charge separation efficiency. Moreover, semiconductor quantum dots as excellent photosensitizers could control absorption spectrum because of their particle radius and high absorption cross-section. Finally, photocatalytic performance of the ternary system is superior to that of the binary system and pure Ti-MOFs. Among the limited Ti-MOFs, only two typical Ti-MOF (MIL-125 and $NH_2$-MIL-125) based composites have been intensively investigated. Thus, photocatalytic applications of Ti-MOF composites should be further extended to other Ti-MOFs. Meanwhile, new Ti-MOFs with lower energy band and higher energy transfer efficiency are needed to be further developed.

In terms of photocatalytic applications of Ti-MOFs, the unique $Ti^{4+}/Ti^{3+}$ reversible redox conversion upon light illumination together with excellent thermal/chemical stability and reusability in aqueous and organic systems grands Ti-MOFs great potentials in a wide range of photo-driven catalytic redox reactions. While efforts to expand their applications are much needed, one ultimate target using this emerging class of porous materials should be efficient utilization of solar energy *via* their unique photoactive Ti-based moieties with the extension of light absorption to visible and near infrared region. The bandgap of Ti-MOFs could be engineered by functionalization of ligands and development of new structures, while the

catalytic activity could be further improved by composition with other highly active species like metal nanoparticles and graphene. Among the limited Ti-MOFs, MIL-125 and $NH_2$-MIL-125 have attracted special attention due to their high stability and effective photocatalytic activity. In addition to these two typical Ti-MOFs, photocatalytic applications should be further extended to other Ti-MOFs. Meanwhile, new Ti-MOFs and Ti-MOF based composites with well-defined textural structure, low bandgap and high energy transfer efficiency should be explored.

**Acknowledgements**

This work is financially supported by the Singapore Academic Research Fund (No. RG112/15, RG19/16, RG121/16, and RG11/17), the Singapore Agency for Science, Technology and Research (A*STAR) AME IRG grant (No. A1783c0007), the National Natural Science Foundation of China (No. 21371014), and the National Program for Support of Top-notch Young Professionals.

**References**

[1] O.M. Yaghi, H. Li, J. Am. Chem. Soc. 117 (1995) 10401-10402.

[2] O.M. Yaghi, G. Li, H. Li, Nature 378 (1995) 703-706.

[3] H. Furukawa, K.E. Cordova, M. O'Keeffe, O.M. Yaghi, Science 341 (2013) 1230444.

[4] Y. Zhao, Chem. Mater. 28 (2016) 8079-8081.

[5] R.E. Morris, L. Brammer, Chem. Soc. Rev. 46 (2017) 5444-5462.

[6] S. Furukawa, J. Reboul, S. Diring, K. Sumida, S. Kitagawa, Chem. Soc. Rev. 43 (2014) 5700-5734.

[7] W. Lu, Z. Wei, Z.-Y. Gu, T.-F. Liu, J. Park, J. Park, J. Tian, M. Zhang, Q. Zhang, T. Gentle III, M. Bosch, H.-C. Zhou, Chem. Soc. Rev. 43 (2014) 5561-5593.

[8] C.M. Doherty, D. Buso, A.J. Hill, S. Furukawa, S. Kitagawa, P. Falcaro, Acc. Chem. Res. 47 (2014) 396-405.

[9] L. Chen, R. Luque, Y. Li, Chem. Soc. Rev. 46 (2017) 4614-4630.

[10] A. Carne, C. Carbonell, I. Imaz, D. Maspoch, Chem. Soc. Rev. 40 (2011) 291-305.

[11] K. Adil, Y. Belmabkhout, R.S. Pillai, A. Cadiau, P.M. Bhatt, A.H. Assen, G. Maurin, M. Eddaoudi, Chem. Soc. Rev. 46 (2017) 3402-3430.

[12] N.A. Ramsahye, P. Trens, C. Shepherd, P. Gonzalez, T.K. Trung, F. Ragon, C. Serre, Microporous Mesoporous Mat. 189 (2014) 222-231.

[13] J. Liu, P.K. Thallapally, B.P. McGrail, D.R. Brown, J. Liu, Chem. Soc. Rev. 41 (2012) 2308-2322.

[14] P.-Z. Li, X.-J. Wang, K. Zhang, A. Nalaparaju, R. Zou, R. Zou, J. Jiang, Y. Zhao, Chem. Commun. 50 (2014) 4683-4685.

[15] P.-Z. Li, Y. Zhao, Chem. Asian J. 8 (2013) 1680-1691.

[16] E. Barea, C. Montoro, J.A.R. Navarro, Chem. Soc. Rev. 43 (2014) 5419-5430.

[17] A. Corma, H. García, F.X. Llabrés i Xamena, Chem. Rev. 110 (2010) 4606-4655.

[18] J. Liu, L. Chen, H. Cui, J. Zhang, L. Zhang, C.-Y. Su, Chem. Soc. Rev. 43 (2014) 6011-6061.

[19] L.-B. Sun, X.-Q. Liu, H.-C. Zhou, Chem. Soc. Rev. 44 (2015) 5092-5147.

[20] S. Wang, X. Wang, Small 11 (2015) 3097-3112.

[21] T. Zhang, W. Lin, Chem. Soc. Rev. 43 (2014) 5982-5993.

[22] S.M.J. Rogge, A. Bavykina, J. Hajek, H. Garcia, A.I. Olivos-Suarez, A. Sepulveda-Escribano, A. Vimont, G. Clet, P. Bazin, F. Kapteijn, M. Daturi, E.V. Ramos-Fernandez, F.X. Llabres i Xamena, V. Van Speybroeck, J. Gascon, Chem. Soc. Rev. 46 (2017) 3134-3184.

[23] J. Liang, Z. Liang, R. Zou, Y. Zhao, Adv. Mater. 29 (2017) 1701139.

[24] R. Medishetty, J.K. Zareba, D. Mayer, M. Samoc, R.A. Fischer, Chem. Soc. Rev. 46 (2017) 4976-5004.

[25] Z. Hu, B.J. Deibert, J. Li, Chem. Soc. Rev. 43 (2014) 5815-5840.

[26] V. Stavila, A.A. Talin, M.D. Allendorf, Chem. Soc. Rev. 43 (2014) 5994-6010.

[27] D. Sheberla, L. Sun, M. Blood-Forsythe, S. Er, C.R. Wade, C.K. Brozek, A. Aspuru-Guzik, M. Dincă, J. Am. Chem. Soc. 136 (2014) 8859-8862.

[28] W.Y. Kim, K.S. Kim, Acc. Chem. Res. 43 (2010) 111-120.

[29] M.G. Campbell, S.F. Liu, T.M. Swager, M. Dincă, J. Am. Chem. Soc. 137 (2015) 13780-13783.

[30] I. Stassen, N. Burtch, A. Talin, P. Falcaro, M. Allendorf, R. Ameloot, Chem. Soc. Rev. 46 (2017) 3185-3241.

[31] B. Chen, S. Xiang, G. Qian, Acc. Chem. Res. 43 (2010) 1115-1124.

[32] X. Chen, C. Li, M. Gratzel, R. Kostecki, S.S. Mao, Chem. Soc. Rev. 41 (2012) 7909-7937.

[33] A. Mahmood, W. Guo, H. Tabassum, R. Zou, Adv. Energy Mater. 6 (2016) 1600423.

[34] H. Wang, Q.-L. Zhu, R. Zou, Q. Xu, Chem 2 (2017) 52-80.

[35] W. Xia, A. Mahmood, R. Zou, Q. Xu, Energy Environ. Sci. 8 (2015) 1837-1866.

[36] P. Horcajada, R. Gref, T. Baati, P.K. Allan, G. Maurin, P. Couvreur, G. Férey, R.E. Morris, C. Serre, Chem. Rev. 112 (2012) 1232-1268.

[37] X. Lian, Y. Fang, E. Joseph, Q. Wang, J. Li, S. Banerjee, C. Lollar, X. Wang, H.-C. Zhou, Chem. Soc. Rev. 46 (2017) 3386-3401.

[38] P. Horcajada, T. Chalati, C. Serre, B. Gillet, C. Sebrie, T. Baati, J.F. Eubank, D. Heurtaux, P. Clayette, C. Kreuz, J.-S. Chang, Y.K. Hwang, V. Marsaud, P.-N. Bories, L. Cynober, S. Gil, G. Férey, P. Couvreur, R. Gref, Nat. Mater. 9 (2010) 172-178.

[39] A.C. McKinlay, R.E. Morris, P. Horcajada, G. Férey, R. Gref, P. Couvreur, C. Serre, Angew. Chem. Int. Ed. 49 (2010) 6260-6266.

[40] T. Devic, C. Serre, Chem. Soc. Rev. 43 (2014) 6097-6115.

[41] M.A. Nasalevich, C.H. Hendon, J.G. Santaclara, K. Svane, B. van der Linden, S.L. Veber, M.V. Fedin, A.J. Houtepen, M.A. van der Veen, F. Kapteijn, A. Walsh, J. Gascon, Sci. Rep. 6 (2016) 23676.

[42] A. Erxleben, Coord. Chem. Rev. 246 (2003) 203-228.

[43] Y. Yan, S. Yang, A.J. Blake, M. Schröder, Acc. Chem. Res. 47 (2014) 296-307.

[44] J.Y. Lu, Coord. Chem. Rev. 246 (2003) 327-347.

[45] Y. Cui, B. Chen, G. Qian, Coord. Chem. Rev. 273-274 (2014) 76-86.

[46] C. Pagis, M. Ferbinteanu, G. Rothenberg, S. Tanase, ACS Catal. 6 (2016) 6063-6072.

[47] V. Bon, V. Senkovskyy, I. Senkovska, S. Kaskel, Chem. Commun. 48 (2012) 8407-8409.

[48] A. Schaate, P. Roy, A. Godt, J. Lippke, F. Waltz, M. Wiebcke, P. Behrens, Chem. Eur. J. 17 (2011) 6643-6651.

[49] J. Canivet, A. Fateeva, Y. Guo, B. Coasne, D. Farrusseng, Chem. Soc. Rev. 43 (2014) 5594-5617.

[50] J.J. Low, A.I. Benin, P. Jakubczak, J.F. Abrahamian, S.A. Faheem, R.R. Willis, J. Am. Chem. Soc. 131 (2009) 15834-15842.

[51] J.B. Decoste, G.W. Peterson, M.W. Smith, C.A. Stone, C.R. Willis, J. Am. Chem. Soc. 134 (2012) 1486-1489.

[52] J.G. Nguyen, S.M. Cohen, J. Am. Chem. Soc. 132 (2010) 4560-4561.

[53] S.J. Yang, C.R. Park, Adv. Mater. 24 (2012) 4010-4013.

[54] W. Zhang, Y. Hu, J. Ge, H.-L. Jiang, S.-H. Yu, J. Am. Chem. Soc. 136 (2014) 16978-16981.

[55] P. Horcajada, S. Surble, C. Serre, D.-Y. Hong, Y.-K. Seo, J.-S. Chang, J.-M. Greneche, I. Margiolaki, G. Férey, Chem.Commun. 27(2007) 2820-2822.

[56] O.I. Lebedev, F. Millange, C. Serre, G. Van Tendeloo, G. Férey, Chem. Mater. 17 (2005) 6525-6527.

[57] J.H. Cavka, S. Jakobsen, U. Olsbye, N. Guillou, C. Lamberti, S. Bordiga, K.P. Lillerud, J. Am. Chem. Soc. 130 (2008) 13850-13851.

[58] V. Guillerm, F. Ragon, M. Dan-Hardi, T. Devic, M. Vishnuvarthan, B. Campo, A. Vimont, G. Clet, Q. Yang, G. Maurin, G. Férey, A. Vittadini, S. Gross, C. Serre, Angew. Chem. Int. Ed. 51 (2012) 9267-9271.

[59] G. Mouchaham, L. Cooper, N. Guillou, C. Martineau, E. Elkaïm, S. Bourrelly, P.L. Llewellyn, C. Allain, G. Clavier, C. Serre, T. Devic, Angew. Chem. Int. Ed. 54 (2015) 13297-13301.

[60] Y. Bai, Y. Dou, L.-H. Xie, W. Rutledge, J.-R. Li, H.-C. Zhou, Chem. Soc. Rev. 45 (2016) 2327-2367.

[61] J. Schneider, M. Matsuoka, M. Takeuchi, J. Zhang, Y. Horiuchi, M. Anpo, D.W. Bahnemann, Chem. Rev. 114 (2014) 9919-9986.

[62] W.-H. Fang, J.-F. Wang, L. Zhang, J. Zhang, Chem. Mater. 29 (2017) 2681-2684.

[63] W.-H. Fang, L. Zhang, J. Zhang, J. Am. Chem. Soc. 138 (2016) 7480-7483.

[64] J.-X. Liu, M.-Y. Gao, W.-H. Fang, L. Zhang, J. Zhang, Angew. Chem. Int. Ed. 55 (2016) 5160-5165.

[65] A. Santiago Portillo, H.G. Baldoví, M.T. García Fernandez, S. Navalón, P. Atienzar, B. Ferrer, M. Alvaro, H. Garcia, Z. Li, J. Phys. Chem. C 121 (2017) 7015-7024.

[66] P. Coppens, Y. Chen, E. Trzop, Chem. Rev. 114 (2014) 9645-9661.

[67] L. Rozes, C. Sanchez, Chem. Soc. Rev. 40 (2011) 1006-1030.

[68] M. Dan-Hardi, C. Serre, T. Frot, L. Rozes, G. Maurin, C. Sanchez, G. Férey, J. Am. Chem. Soc. 131 (2009) 10857-10859.

[69] H. Assi, G. Mouchaham, N. Steunou, T. Devic, C. Serre, Chem. Soc. Rev. 46 (2017) 3431-3452.

[70] D. Sun, Z. Li, Chin. J. Chem. 35 (2017) 135-147.

[71] C. Serre, G. Férey, Inorg. Chem. 38 (1999) 5370-5373.

[72] C. Serre, G. Férey, Inorg. Chem. 40 (2001) 5350-5353.

[73] C. Serre, J.A. Groves, P. Lightfoot, A.M.Z. Slawin, P.A. Wright, N. Stock, T. Bein, M. Haouas, F. Taulelle, G. Férey, Chem. Mater. 18 (2006) 1451-1457.

[74] S. Cassaignon, M. Koelsch, J.-P. Jolivet, J. Mater. Sci. 42 (2007) 6689-6695.

[75] J.A. Mason, L.E. Darago, W.W. Lukens, J.R. Long, Inorg. Chem. 54 (2015) 10096-10104.

[76] H. Assi, L.C. Pardo Pérez, G. Mouchaham, F. Ragon, M. Nasalevich, N. Guillou, C. Martineau, H. Chevreau, F. Kapteijn, J. Gascon, P. Fertey, E. Elkaim, C. Serre, T. Devic, Inorg. Chem. 55 (2016) 7192-7199.

[77] S. Yuan, T.-F. Liu, D. Feng, J. Tian, K. Wang, J. Qin, Q. Zhang, Y.-P. Chen, M. Bosch, L. Zou, S.J. Teat, S.J. Dalgarno, H.-C. Zhou, Chem. Sci. 6 (2015) 3926-3930.

[78] H.L. Nguyen, F. Gándara, H. Furukawa, T.L.H. Doan, K.E. Cordova, O.M. Yaghi, J. Am. Chem. Soc. 138 (2016) 4330-4333.

[79] H.L. Nguyen, T.T. Vu, D. Le, T.L.H. Doan, V.Q. Nguyen, N.T.S. Phan, ACS Catal. 7 (2017) 338-342.

[80] S. Hu, M. Liu, K. Li, Y. Zuo, A. Zhang, C. Song, G. Zhang, X. Guo, CrystEngComm 16 (2014) 9645-9650.

[81] Y. Fu, Y. Liu, Z. Shi, B. Li, W. Pang, J. Solid State Chem. 163 (2002) 427-435.

[82] C. Zlotea, D. Phanon, M. Mazaj, D. Heurtaux, V. Guillerm, C. Serre, P. Horcajada, T. Devic, E. Magnier, F. Cuevas, G. Férey, P.L. Llewellyn, M. Latroche, Dalton Trans. 40 (2011) 4879-4881.

[83] J. Gao, J. Miao, P.-Z. Li, W.Y. Teng, L. Yang, Y. Zhao, B. Liu, Q. Zhang, Chem. Commun. 50 (2014) 3786-3788.

[84] N.T.T. Nguyen, H. Furukawa, F. Gándara, C.A. Trickett, H.M. Jeong, K.E. Cordova, O.M. Yaghi, J. Am. Chem. Soc. 137 (2015) 15394-15397.

[85] B. Bueken, F. Vermoortele, D.E.P. Vanpoucke, H. Reinsch, C.-C. Tsou, P. Valvekens, T. De Baerdemaeker, R. Ameloot, C.E.A. Kirschhock, V. Van Speybroeck, J.M. Mayer, D. De Vos, Angew. Chem. 127 (2015) 14118-14123.

[86] K. Hong, W. Bak, H. Chun, Inorg. Chem. 52 (2013) 5645-5647.

[87] K. Hong, H. Chun, Chem. Commun. 49 (2013) 10953-10955.

[88] S.-N. Kim, J. Kim, H.-Y. Kim, H.-Y. Cho, W.-S. Ahn, Catal. Today 204 (2013) 85-93.

[89] P. George, N.R. Dhabarde, P. Chowdhury, Mater. Lett. 186 (2017) 151-154.

[90] Y. Han, L. Han, L. Zhang, S. Dong, J. Mater. Chem. A 3 (2015) 14669-14674.

[91] Y.-R. Lee, S.-M. Cho, S.-H. Baeck, W.-S. Ahn, W.-S. Cho, RSC Adv. 6 (2016) 63286-63290.

[92] S.-Y. Ding, W. Wang, Chem. Soc. Rev. 42 (2013) 548-568.

[93] X. Feng, X. Ding, D. Jiang, Chem. Soc. Rev. 41 (2012) 6010-6022.

[94] A. Mallick, B. Garai, D.D. Díaz, R. Banerjee, Angew. Chem. 125 (2013) 14000-14004.

[95] J.-R. Li, H.-C. Zhou, Nature Chem. 2 (2010) 893-898.

[96] D.J. Tranchemontagne, Z. Ni, M. O'Keeffe, O.M. Yaghi, Angew. Chem. Int. Ed. 47 (2008) 5136-5147.

[97] J.D. Evans, C.J. Sumby, C.J. Doonan, Chem. Soc. Rev. 43 (2014) 5933-5951.

[98] C.K. Brozek, M. Dincă, Chem. Soc. Rev. 43 (2014) 5456-5467.

[99] M. Kim, J.F. Cahill, H. Fei, K.A. Prather, S.M. Cohen, J. Am. Chem. Soc. 134 (2012) 18082-18088.

[100] C. Hon Lau, R. Babarao, M.R. Hill, Chem. Commun. 49 (2013) 3634-3636.

[101] Y. Lee, S. Kim, J.K. Kang, S.M. Cohen, Chem. Commun. 51 (2015) 5735-5738.

[102] S.J.D. Smith, B.P. Ladewig, A.J. Hill, C.H. Lau, M.R. Hill, Sci. Rep. 5 (2015) 7823.

[103] A.M. Rasero-Almansa, M. Iglesias, F. Sanchez, RSC Adv. 6 (2016) 106790-106797.

[104] L. Zou, D. Feng, T.-F. Liu, Y.-P. Chen, S. Yuan, K. Wang, X. Wang, S. Fordham, H.-C. Zhou, Chem. Sci. 7 (2016) 1063-1069.

[105] T.-F. Liu, L. Zou, D. Feng, Y.-P. Chen, S. Fordham, X. Wang, Y. Liu, H.-C. Zhou, J. Am. Chem. Soc. 136 (2014) 7813-7816.

[106] N.D. McNamara, J.C. Hicks, ACS Appl. Mater. Inter. 7 (2015) 5338-5346.

[107] R.M. Abdelhameed, M.M.Q. Simões, A.M.S. Silva, J. Rocha, Chem. Eur. J. 21 (2015) 11072-11081.

[108] H. Guo, D. Guo, Z. Zheng, W. Weng, J. Chen, Appl. Organometal. Chem. 29 (2015) 618-623.

[109] L. Shen, M. Luo, L. Huang, P. Feng, L. Wu, Inorg. Chem. 54 (2015) 1191-1193.

[110] M. Martis, W. Meicheng, K. Mori, H. Yamashita, Catal. Today 235 (2014) 98-102.

[111] M. Martis, K. Mori, K. Fujiwara, W.-S. Ahn, H. Yamashita, J. Phys. Chem. C 117 (2013) 22805-22810.

[112] P. Puthiaraj, W.-S. Ahn, Catal. Commun. 65 (2015) 91-95.

[113] Y. Fu, L. Sun, H. Yang, L. Xu, F. Zhang, W. Zhu, Appl. Catal. B-Environ. 187 (2016) 212-217.

[114] H. Wang, X. Yuan, Y. Wu, X. Chen, L. Leng, G. Zeng, RSC Adv. 5 (2015) 32531-32535.

[115] H. Wang, X. Yuan, Y. Wu, G. Zeng, X. Chen, L. Leng, H. Li, Appl. Catal. B-Environ. 174-175 (2015) 445-454.

[116] J. Xu, S. He, H. Zhang, J. Huang, H. Lin, X. Wang, J. Long, J. Mater. Chem. A 3 (2015) 24261-24271.

[117] D. Jin, Q. Xu, L. Yu, X. Hu, Microchim. Acta 182 (2015) 1885-1892.

[118] A.V. Vinogradov, H. Zaake-Hertling, E. Hey-Hawkins, A.V. Agafonov, G.A. Seisenbaeva, V.G. Kessler, V.V. Vinogradov, Chem. Commun. 50 (2014) 10210-10213.

[119] Y. Yoshida, Y. Izumi, J. Catal. 332 (2015) 1-12.

[120] C. Serre, F. Taulelle, G. Férey, Chem. Commun. (2003) 2755-2765.

[121] V. Benoit, R.S. Pillai, A. Orsi, P. Normand, H. Jobic, F. Nouar, P. Billemont, E. Bloch, S. Bourrelly, T. Devic, P.A. Wright, G. de Weireld, C. Serre, G. Maurin, P.L. Llewellyn, J. Mater. Chem. A 4 (2016) 1383-1389.

[122] P.G. Yot, K. Yang, F. Ragon, V. Dmitriev, T. Devic, P. Horcajada, C. Serre, G. Maurin, Dalton Trans. 45 (2016) 4283-4288.

[123] K. Gigant, A. Rammal, M. Henry, J. Am. Chem. Soc. 123 (2001) 11632-11637.

[124] H. Chun, Bull. Korean Chem. Soc. 35 (2014) 1879-1882.

[125] W. Liu, J. Cai, Z. Ding, Z. Li, Appl. Catal. B-Environ. 174-175 (2015) 421-426.

[126] H. Hou, M. Shang, F. Gao, L. Wang, Q. Liu, J. Zheng, Z. Yang, W. Yang, ACS Appl. Mater. Inter. 8 (2016) 20128-20137.

[127] N. Qin, Y. Liu, W. Wu, L. Shen, X. Chen, Z. Li, L. Wu, Langmuir 31 (2015) 1203-1209.

[128] Y. Fu, D. Sun, Y. Chen, R. Huang, Z. Ding, X. Fu, Z. Li, Angew. Chem. 124 (2012) 3420-3423.

[129] M.R. Hoffmann, S.T. Martin, W. Choi, D.W. Bahnemann, Chem. Rev. 95 (1995) 69-96.

[130] C.H. Hendon, D. Tiana, M. Fontecave, C. Sanchez, L. D'arras, C. Sassoye, L. Rozes, C. Mellot-Draznieks, A. Walsh, J. Am. Chem. Soc. 135 (2013) 10942-10945.

[131] M.A. Nasalevich, M.G. Goesten, T.J. Savenije, F. Kapteijn, J. Gascon, Chem. Commun. 49 (2013) 10575-10577.

[132] J.G. Santaclara, M.A. Nasalevich, S. Castellanos, W.H. Evers, F.C.M. Spoor, K. Rock, L.D.A. Siebbeles, F. Kapteijn, F. Grozema, A. Houtepen, J. Gascon, J. Hunger, M.A. van der Veen, ChemSusChem 9 (2016) 388-395.

[133] M. de Miguel, F. Ragon, T. Devic, C. Serre, P. Horcajada, H. García, ChemPhysChem 13 (2012) 3651-3654.

[134] G.N. Schrauzer, T.D. Guth, J. Am. Chem. Soc. 99 (1977) 7189-7193.

[135] M. Fujihira, Y. Satoh, T. Osa, Nature 293 (1981) 206-208.

[136] D. Sun, W. Liu, Y. Fu, Z. Fang, F. Sun, X. Fu, Y. Zhang, Z. Li, Chem. Eur. J. 20 (2014) 4780-4788.

[137] Y. Horiuchi, T. Toyao, M. Saito, K. Mochizuki, M. Iwata, H. Higashimura, M. Anpo, M. Matsuoka, J. Phys. Chem. C 116 (2012) 20848-20853.

[138] D. Sun, L. Ye, Z. Li, Appl. Catal. B-Environ. 164 (2015) 428-432.

[139] K. Meyer, M. Ranocchiari, J.A. van Bokhoven, Energy Environ. Sci. 8 (2015) 1923-1937.

[140] M.A. Nasalevich, R. Becker, E.V. Ramos-Fernandez, S. Castellanos, S.L. Veber, M.V. Fedin, F. Kapteijn, J.N.H. Reek, J.I. van der Vlugt, J. Gascon, Energy Environ. Sci. 8 (2015) 364-375.

[141] K. Meyer, S. Bashir, J. Llorca, H. Idriss, M. Ranocchiari, J.A. van Bokhoven, Chem. Eur. J. 22(2016) 13894–13899.

[142] Z. Wu, X. Yuan, J. Zhang, H. Wang, L. Jiang, G. Zeng, ChemCatChem 9 (2017) 41-64.

[143] C.-C. Wang, J.-R. Li, X.-L. Lv, Y.-Q. Zhang, G. Guo, Energy Environ. Sci. 7 (2014) 2831-2867.

[144] E.A. Kozlova, V.N. Panchenko, Z. Hasan, N.A. Khan, M.N. Timofeeva, S.H. Jhung, Catal. Today 266 (2016) 136-143.

[145] A. Dhakshinamoorthy, A.M. Asiri, H. García, Angew. Chem. Int. Ed. 55 (2016) 5414-5445.

[146] X. Yuan, H. Wang, Y. Wu, G. Zeng, X. Chen, L. Leng, Z. Wu, H. Li, Appl. Organometal. Chem. 30 (2016) 289-296.

[147] H. Wang, X. Yuan, Y. Wu, G. Zeng, H. Dong, X. Chen, L. Leng, Z. Wu, L. Peng, Appl. Catal. B-Environ. 186 (2016) 19-29.

[148] S.-R. Zhu, P.-F. Liu, M.-K. Wu, W.-N. Zhao, G.-C. Li, K. Tao, F.-Y. Yi, L. Han, Dalton Trans. 45 (2016) 17521-17529.

[149] J. Li, X. Xu, X. Liu, W. Qin, M. Wang, L. Pan, J. Alloy. Compd. 690 (2017) 640-646.

[150] J. Li, X. Xu, X. Liu, W. Qin, L. Pan, Ceram. Int. 43 (2017) 835-840.

[151] S. Abedi, A. Morsali, New J. Chem. 39 (2015) 931-937.

[152] L.E. Kreno, K. Leong, O.K. Farha, M. Allendorf, R.P. Van Duyne, J.T. Hupp, Chem. Rev. 112 (2012) 1105-1125.

[153] Y. Zhang, B. Fu, K. Liu, Y. Zhang, X. Li, S. Wen, Y. Chen, S. Ruan, Sensor. Actuat. B-Chem. 201 (2014) 281-285.

[154] Q. Xu, Y. Wang, G. Jin, D. Jin, K. Li, A. Mao, X. Hu, Sensor. Actuat. B-Chem. 201 (2014) 274-280.

[155] X. Lian, B. Yan, Inorg. Chem. 55 (2016) 11831-11838.

[156] Z.H. Rada, H.R. Abid, J. Shang, Y. He, P. Webley, S. Liu, H. Sun, S. Wang, Fuel 160 (2015) 318-327.

[157] M.J. Regufe, J. Tamajon, A.M. Ribeiro, A. Ferreira, U.H. Lee, Y.K. Hwang, J.-S. Chang, C. Serre, J.M. Loureiro, A.E. Rodrigues, Energy Fuels 29 (2015) 4654-4664.

[158] S. Vaesen, V. Guillerm, Q. Yang, A.D. Wiersum, B. Marszalek, B. Gil, A. Vimont, M. Daturi, T. Devic, P.L. Llewellyn, C. Serre, G. Maurin, G. De Weireld, Chem. Commun. 49 (2013) 10082-10084.

[159] M. Waqas Anjum, B. Bueken, D. De Vos, I.F.J. Vankelecom, J. Membrane Sci. 502 (2016) 21-28.

[160] S. Friebe, A. Mundstock, D. Unruh, F. Renz, J. Caro, J. Membrane Sci. 516 (2016) 185-193.

[161] M.A. Moreira, J.C. Santos, A.F.P. Ferreira, J.M. Loureiro, F. Ragon, P. Horcajada, P.G. Yot, C. Serre, A.E. Rodrigues, Langmuir 28 (2012) 3494-3502.

[162] S. Van der Perre, A. Liekens, B. Bueken, D.E. De Vos, G.V. Baron, J.F.M. Denayer, J. Chromatogra. A 1469 (2016) 68-76.

[163] H.-Y. Kim, S.-N. Kim, J. Kim, W.-S. Ahn, Mater. Res. Bull. 48 (2013) 4499-4505.

[164] B. Li, J. Liu, Z. Nie, W. Wang, D. Reed, J. Liu, P. McGrail, V. Sprenkle, Nano Lett. 16 (2016) 4335-4340.

[165] Z. Wang, X. Li, H. Xu, Y. Yang, Y. Cui, H. Pan, Z. Wang, B. Chen, G. Qian, J. Mater. Chem. A 2 (2014) 12571-12575.

[166] Z. Xiu, M.H. Alfaruqi, J. Gim, J. Song, S. Kim, P.T. Duong, J.P. Baboo, V. Mathew, J. Kim, J. Alloys Compd. 674 (2016) 174-178.

[167] X. Shi, Z. Zhang, K. Du, Y. Lai, J. Fang, J. Li, J. Power Sources 330 (2016) 1-6.

[168] W.S. Chi, D.K. Roh, C.S. Lee, J.H. Kim, J. Mater. Chem. A 3 (2015) 21599-21608.

[169] I. D. Ivanchikova, J. S. Lee, N. V. Maksimchuk, A. N. Shmakov, Y. A. Chesalov, A. B. Ayupov, Y. K. Hwang, C.-H. Jun, J.-S. Chang, O. A. Kholdeeva, Eur. J. Inorg. Chem. 2014 (2014) 132-139.

[170] N. D. McNamara, J. Kim, J. C. Hicks, Energy Fuels 30 (2016) 594-602.

[171] N. D. McNamara, G. T. Neumann, E. T. Masko, J. A. Urban, J. C. Hicks, J. Catal. 305 (2013) 217-226.

[172] F.-Q. Liu, T. Don Tilley, Chem. Commun. (1998) 103-104.

**Table 1.** Synthetic methods of some reported Ti-MOFs discussed in this review.

| Ti-MOF | Formula | Ti precursor | Ligand(L) | Solvent | Synthesis | Ref. |
|---|---|---|---|---|---|---|
| MIL-22 | $Ti_3O_2(H_2O)_2(O_3P\text{-}(CH_2)\text{-}PO_3)_2\bullet(H_2O)_2$ | Hydrous $TiO_2$ | Methylenediphosphonate | HF (40 %)+$H_2O$ | 4 d, 493 K | [71] |
| MIL-25$_2$ | $Ti(O_3P\text{-}(CH_2)_2\text{-}PO_3)$ | Hydrous $TiO_2$ | Ethylenediphosphonate | HF (40 %)+$H_2O$ | 4 d, 463 K | [72] |
| MIL-25$_3$ | $Ti(O_3P\text{-}(CH_2)_3\text{-}PO_3)$ | Hydrous $TiO_2$ | Propylenediphosphonate | HF (40 %)+$H_2O$ | 4 d, 463 K | [72] |
| MIL-91(Ti) | $TiO(H_2L)\bullet nH_2O$ (n ~ 4.5) | Hydrous $TiO_2$ | $H_4L$ | HF (40 %)+$H_2O$ | 4 d, 493 K | [73] |
| Ti-OX | $Ti_4O_4(C_2O_4)_7\bullet 3C_4N_2H_{12}\bullet 2H_2O$ | TBOT | Ethylenediamine + piperazine | Oxalic acid +$H_2O$ | 3 d, 393K | [81] |
| MIL-125 | $Ti_8O_8(OH)_4\text{-}(O_2C\text{-}C_6H_4\text{-}CO_2)_6$ | $Ti(OiPr)_4$ | Terephthalic acid | DMF+MeOH | 15 h, 423 K | [68] |
| $NH_2$-MIL-125 | $Ti_8O_8(OH)_4\text{-}(O_2C\text{-}C_6H_4(NH_2)\text{-}CO_2)_6$ | $Ti(OiPr)_4$ | 2-aminoterephthalic acid | DMF+MeOH | 16 h, 423 K | [82] |
| COK-69 | $[Ti^{IV}{}_3\text{-}(\mu_3\text{-}O)(O)_2(cdc)\bullet DMF]_n$ | $Cp_2Ti^{IV}Cl_2$ | $H_2cdc$ | DMF + acetic acid | 48 h, 383 K | [85] |
| PCN-22 | $Ti_7O_6(L)_{12}\bullet 2DEF$ | $Ti(OiPr)_4$ | TCPP | DEF + benzoic acid | 48 h, 423 K | [77] |
| MOF-901 | $Ti_6O_6(OMe)_6(C_{20}H_{14}N_2(CO_2)_2)_3$ | $Ti(OiPr)_4$ | BDA | MeOH | 3 d, 398 K | [78] |
| MOF-902 | $Ti_6O_6(OMe)_6(C_{26}H_{18}N_2(CO_2)_2)_3$ | $Ti(OiPr)_4$ | BPDA+ 4-aminobenzoic acid | MeOH | 3 d, 413 K | [79] |
| Ti-MIL-101 | $Ti^{III}{}_3O(OEt)(bdc)_3(DMF)_2$ | $TiCl_3$ | $H_2bdc$ | DMF+EtOH | 18 h, 393 K | [75] |
| ZTOF-1 | $[H_2N(CH_3)_2][Zn_3(OH)Ti(obdc)_3(HCO_2)]$ | $Ti(OiPr)_4$ | 2-hydroxyterephthalic acid | DMF | 24 h, 363 K | [86] |
| ZTOF-2 | $[Zn_6Ti_2(ondc)_6(dabco)(CO_3)(OH_2)_3](DMF)_3$ | $Ti(OiPr)_4$ | $H_3ondc$ + dabco | DMF | 1 d, 353 K | [87] |
| NTU-9 | $Ti_2(DOBDC)_3$ | $Ti(OiPr)_4$ | $H_4DOBDC$ | Acetic acid | 5 d, 393 K | [83] |
| NTU-9-like | $Ti(HxDOBDC)_{1.5}(DEAH)_y\bullet nDEF$ | $Ti(OiPr)_4$ | $H_4DOBDC$ | DEF | 20 h, 473 K | [76] |
| MIL-167 | $Ti(DOBDC)_{1,5}(DEAH)_2\bullet nH_2O$ | $Ti(OiPr)_4$ | $H_4DOBDC$ | DEF+MeOH | 24 h, 453 K | [76] |
| MIL-168 | $Ti(DOBDC)(cat)(DEAH)_2$ | $Ti(OiPr)_4$ | $H_4DOBDC$ | DEF+Catechol | 48 h, 453 K | [76] |
| MIL-169 | $TiO_{0.5}(DOBDC)(H_2O)(pipH_2)_{0.5}\bullet H_2O$ | $Ti_4O_4(ox)_7$ $(pipH_2)_3\bullet 2H_2O$ | $H_4DOBDC$ | $H_2O$+Catechol | 72 h, 423 K | [76] |
| Ti-CAT-5 | $Ti(THO)(Me_2NH_2)_2(C_3H_7OH)_{0.06}(DMF)_{0.06}(CH_3CN)_{0.04}H_2O$ | $Ti(OiPr)_4$ | $H_6THO$ + $NBu_4Br$ | DMF | 48 h, 453 K | [84] |

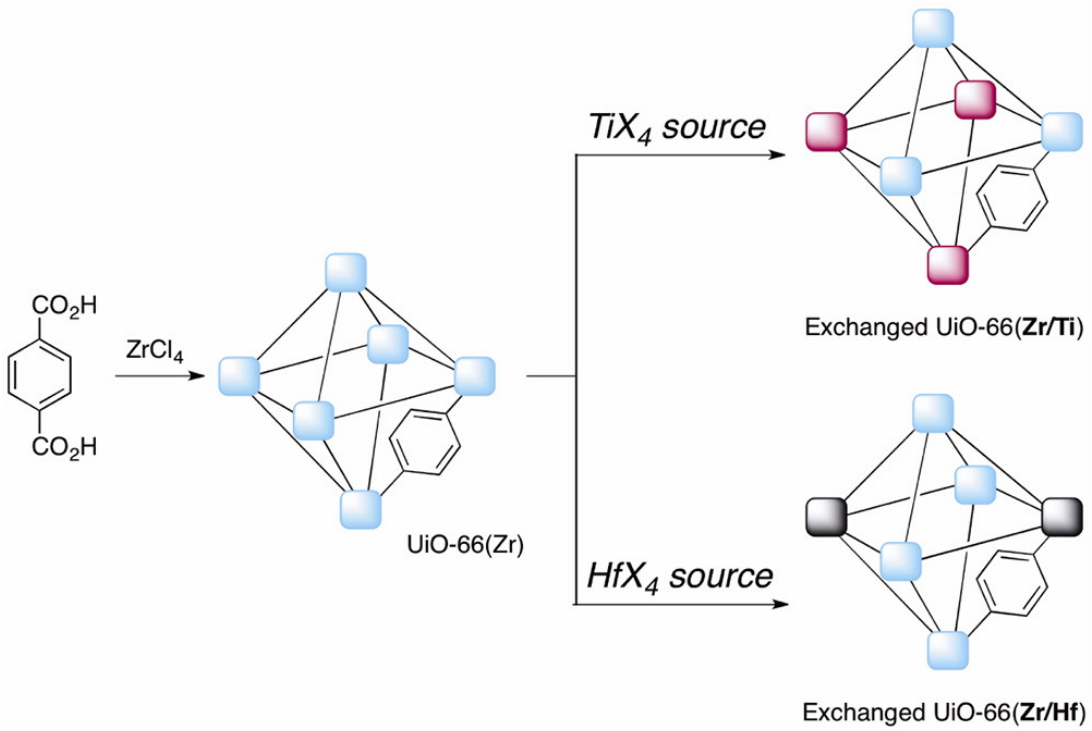


**Figure 1.** Postsynthetic Ti(IV) cation exchange in UiO-66. Adapted with permission from Ref. [99]. Copyright 2012, American Chemical Society.

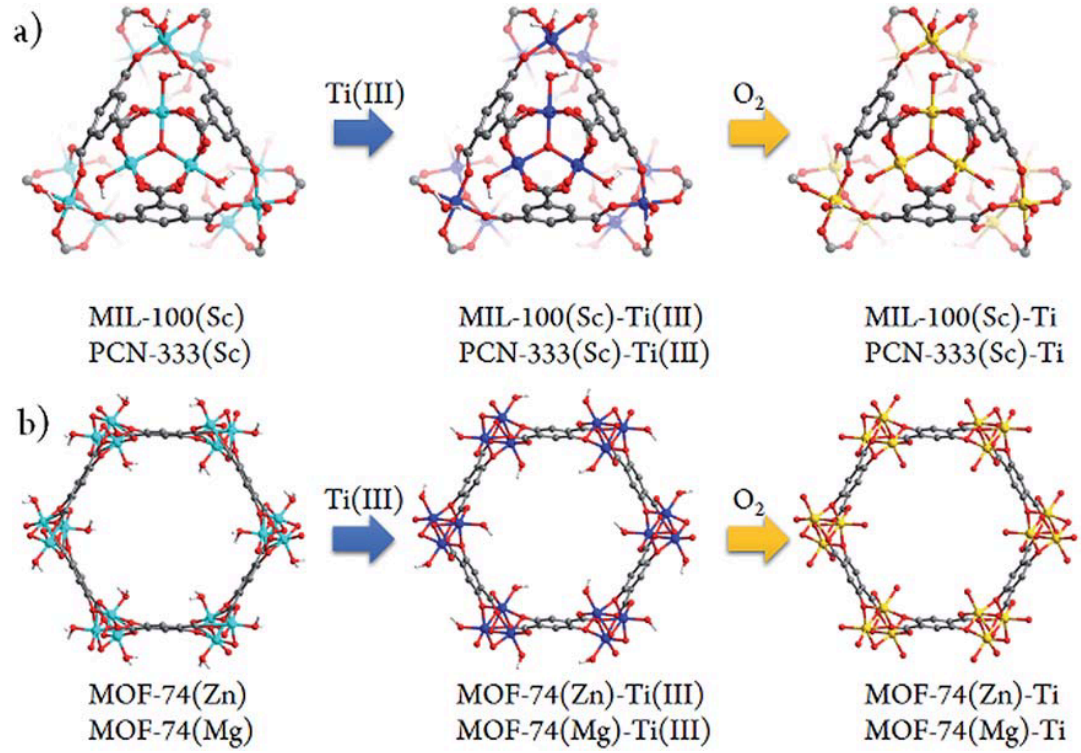


**Figure 2.** Stepwise HVMO procedure for the design of Ti-MOFs from the template MOFs. Adapted with permission from Ref. [104]. Copyright 2016, The Royal Society of Chemistry.

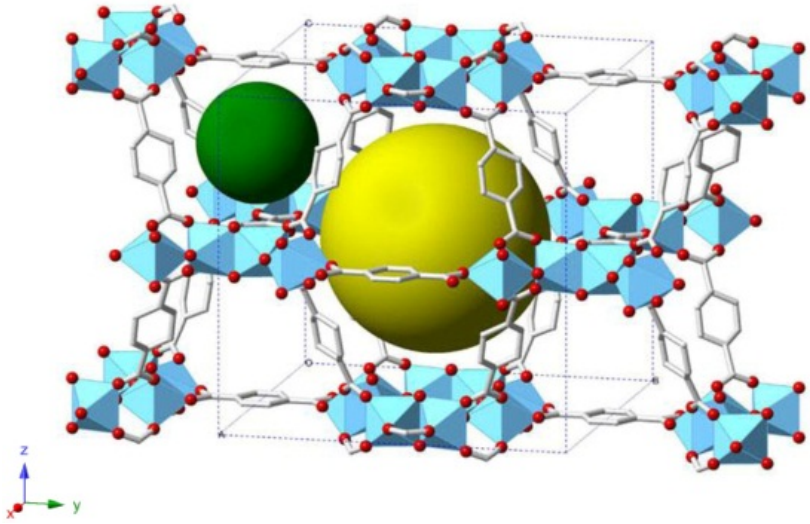

**Figure 3.** Schematic view of octahedral (yellow) and tetrahedral (green) cages of the MIL-125 structure. Adapted with permission from Ref. [68, 88]. Copyright 2012, Elsevier B.V.

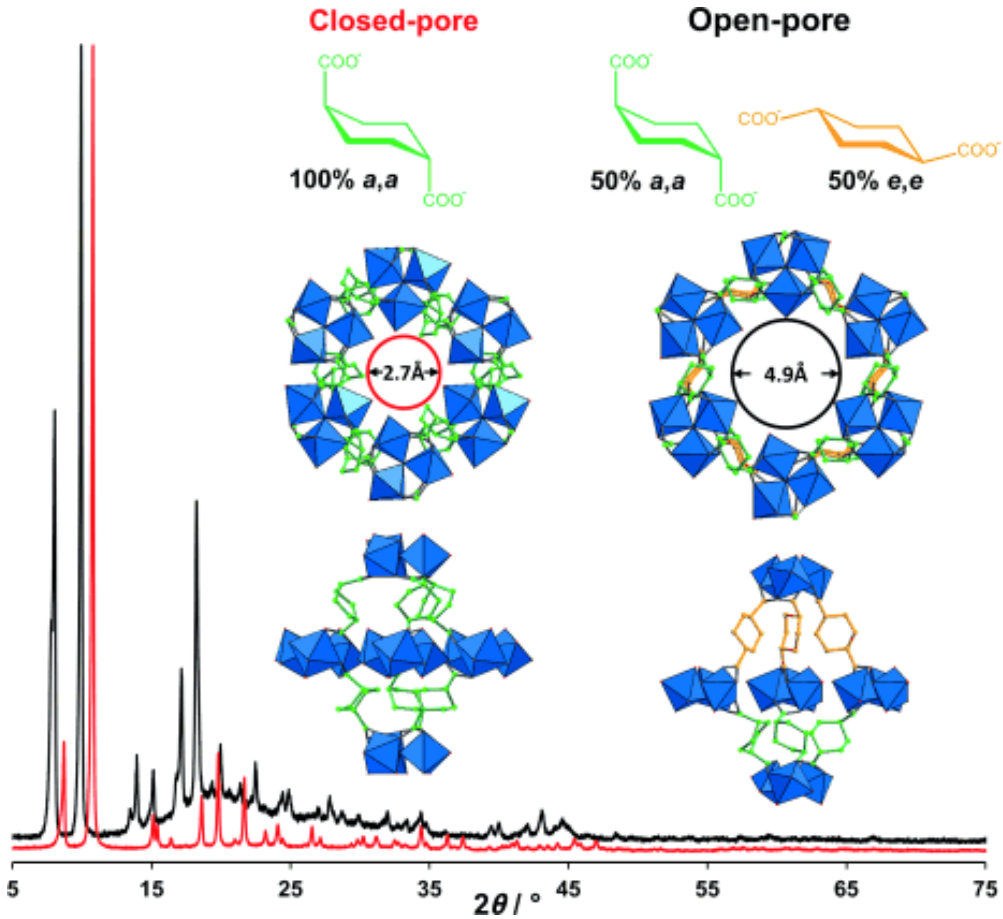


**Figure 4.** Powder XRD patterns and structures of COK-69close (red) and COK-69open (black). COK-69open contains $cdc^{2-}$ linkers in both the *e*,*e*′ and *a*,*a*′ conformation in a 1:1 ratio, whereas COK-69close has only *a*,*a*′-$cdc^{2-}$. Adapted with permission from Ref. [85]. Copyright 2015, WILEY-VCH Verlag GmbH & Co. KGaA, Weinheim.

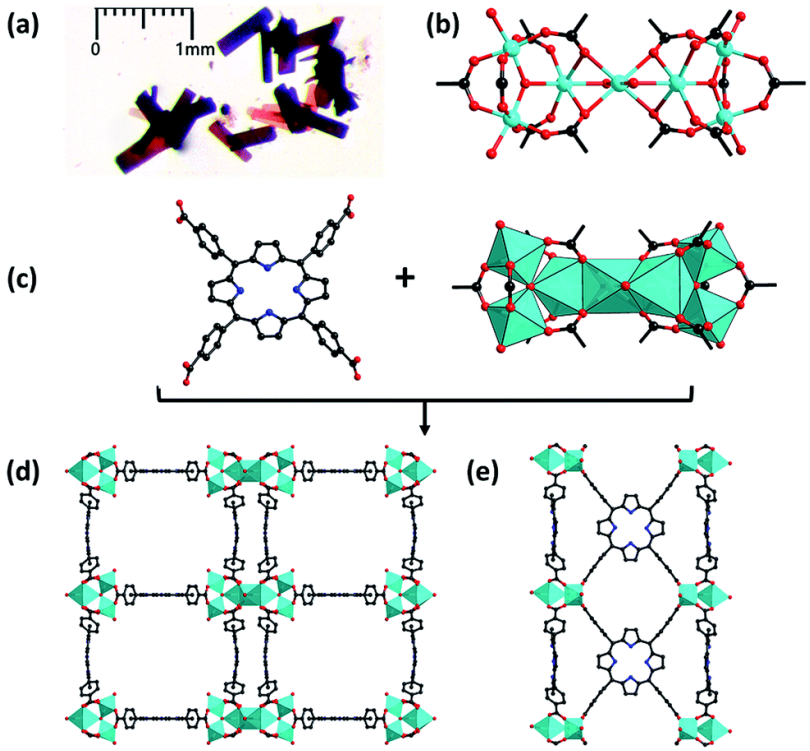


**Figure 5.** (a) Microscope image of PCN-22 crystals. (b) Structure of the $Ti_7O_6$ cluster. (c) Structures of tetratopic TCPP linker (left) and 12-connected $Ti_7O_6$ cluster (right). Structure views of PCN-22 along (d) *a* axis and (e) *b* axis. Adapted with permission from Ref. [77]. Copyright 2015, Royal Society of Chemistry.

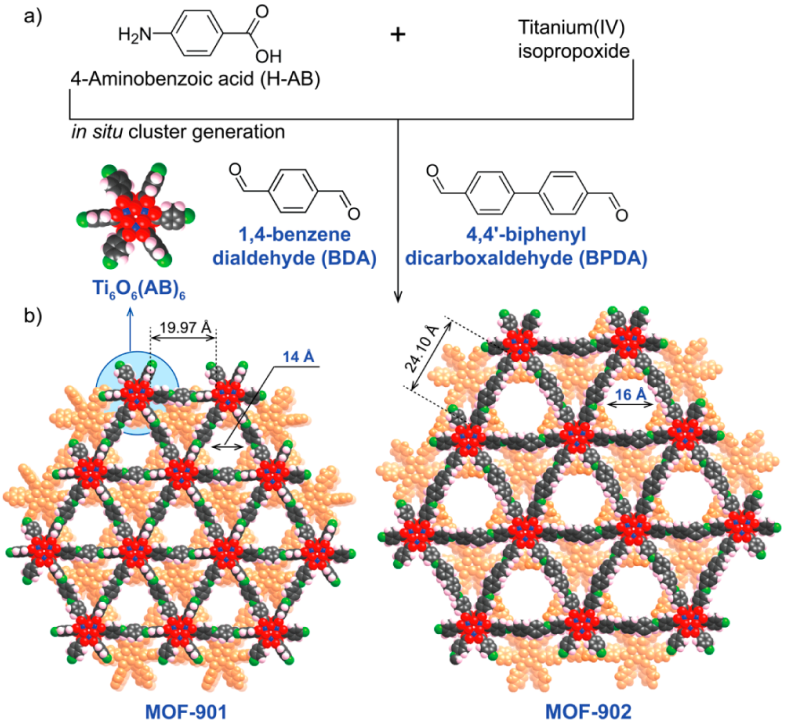


**Figure 6.** Synthetic procedure of MOF-901 and MOF-902. (a) *In situ* Ti−oxo cluster generation. (b) Space filling models for crystal structures of MOF-901 and MOF-902. Adapted with permission from Ref. [79]. Copyright 2017, American Chemical Society.

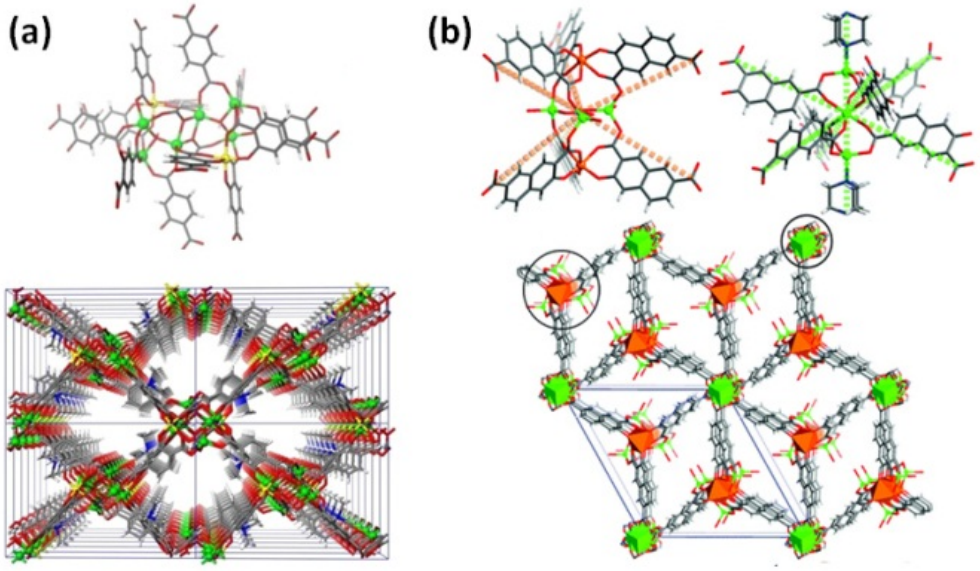


**Figure 7.** (a) $Zn_6Ti_2$ SBU (upper) and overall network viewed along *a* axis (lower) for ZTOF-1. Adapted with permission from Ref. [86]. Copyright (2013) American Chemical Society. (b) 6-connecting trigonal prism and 8-connected pinwheel SBUs (upper) and overall network viewed along the c axis (lower) for ZTOF-2. Adapted with permission from Ref. [87]. Copyright 2013, Royal Society of Chemistry.

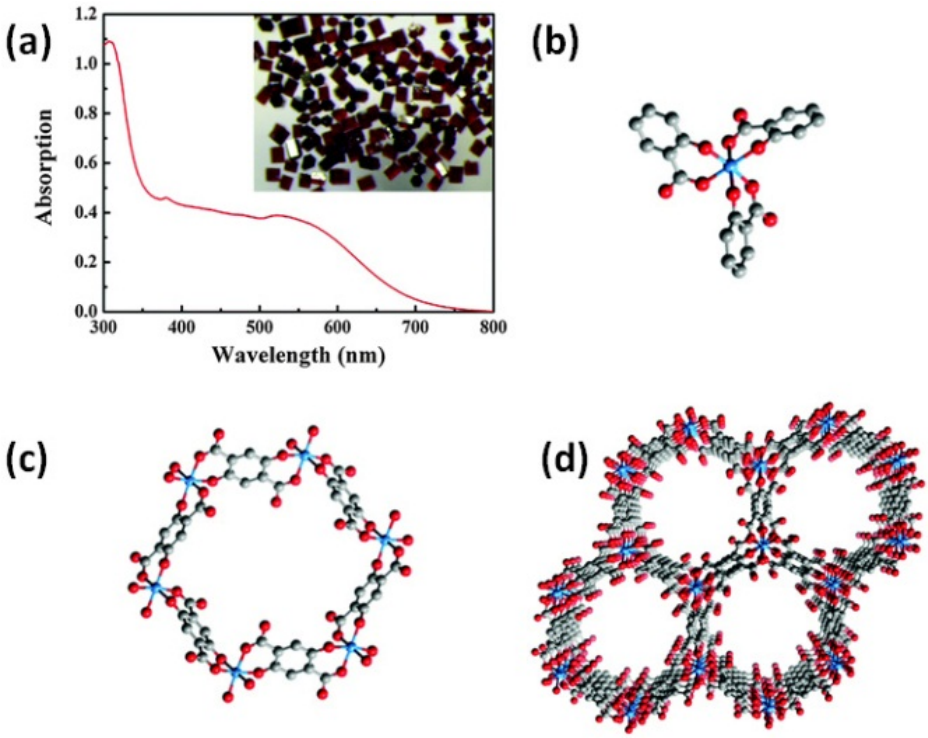


**Figure 8.** (a) Diffuse reflectance spectra and crystals of NTU-9. (b) Coordination mode of the Ti atom in NTU-9. (c) Coordination of the DOBDC ligand in NTU-9. (d) One-dimensional channels of NTU-9 viewed along the *c* axis. Adapted with permission from Ref. [83]. Copyright 2014, Royal Society of Chemistry.

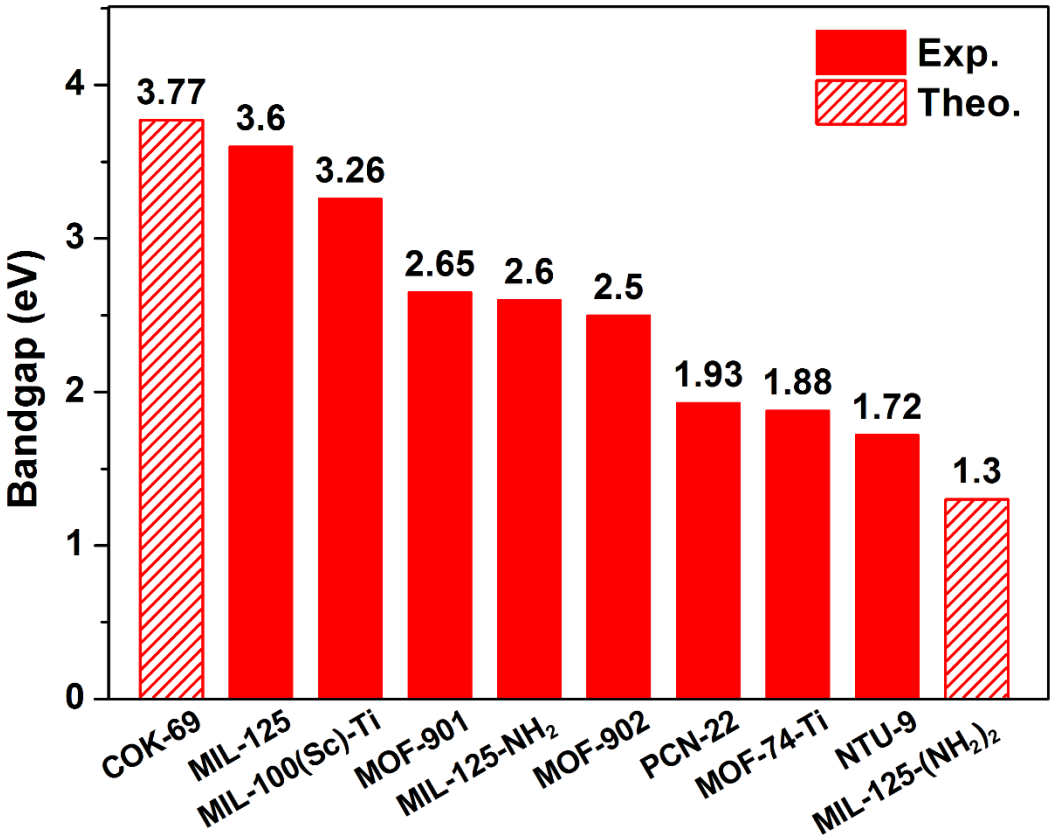


**Figure 9.** Bandgap of Ti-MOFs.

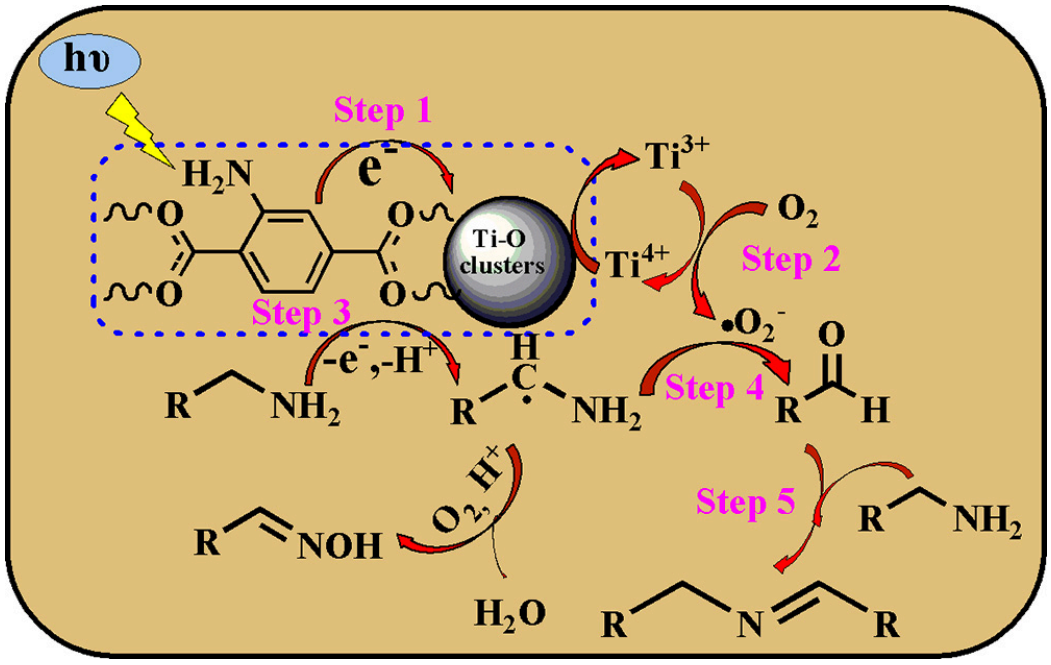


**Figure 10.** Proposed mechanism of the photocatalytic oxidation of amines to imines over $NH_2$-MIL-125. Adapted with permission from Ref. [138]. Copyright 2014, Elsevier B.V.

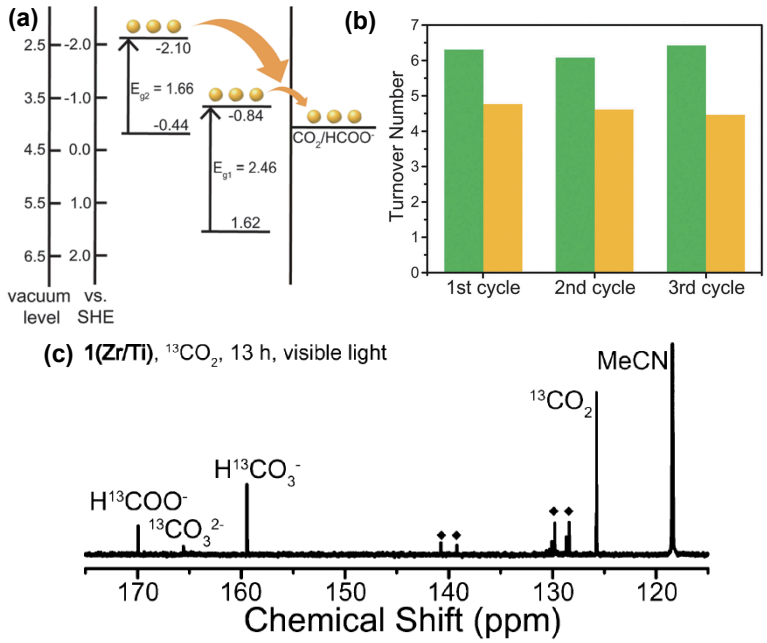


**Figure 11.** (a) Two energy band structure in **1(Zr/Ti)**, which potentially catalyze $CO_2$. (b) Turnover numbers of **1(Zr/Ti)** (green) and UiO-66(Zr/Ti)-$NH_2$ (gold) for photocatalysis of $CO_2$ to HCOOH over three cycles. (c) $^{13}C$ NMR spectrum of the product solution from the photocatalysis of $^{13}CO_2$ by **1(Zr/Ti)** under visible light irradiation for 13 hours. Adapted with permission from Ref. [101]. Copyright 2015, Royal Society of Chemistry.

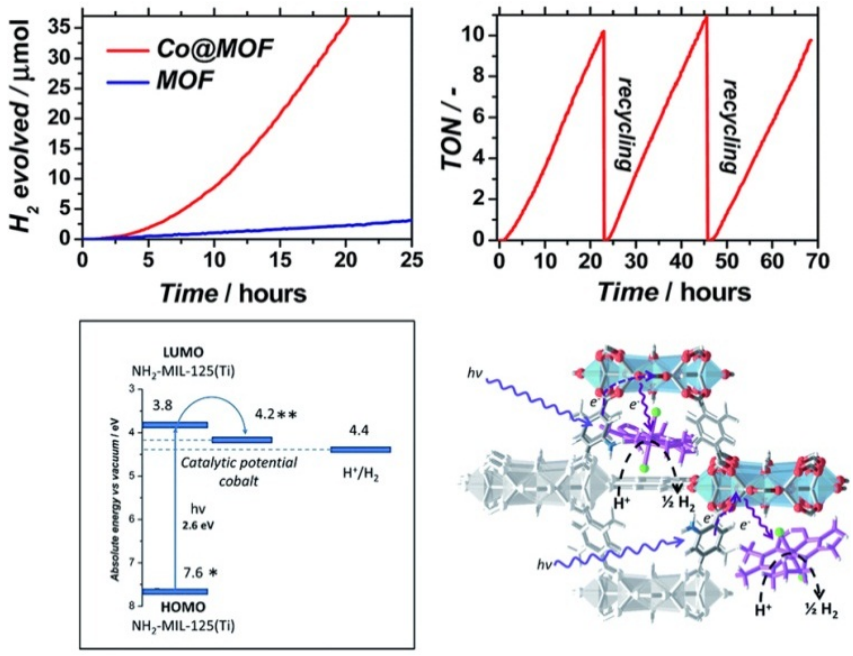


**Figure 12.** (a) Photocatalytic proton reduction using $NH_2$-MIL-125 (blue) and Co@$NH_2$-MIL-125 (red). (b) Recycling tests for Co@$NH_2$-MIL-125. (c) Schematic diagram of redox potentials for components of Co@$NH_2$-MIL-125. (d) Schematic diagram of photocatalytic $H_2$ production over Co@$NH_2$-MIL-125. Adapted with permission from Ref. [140]. Copyright 2014, Royal Society of Chemistry.

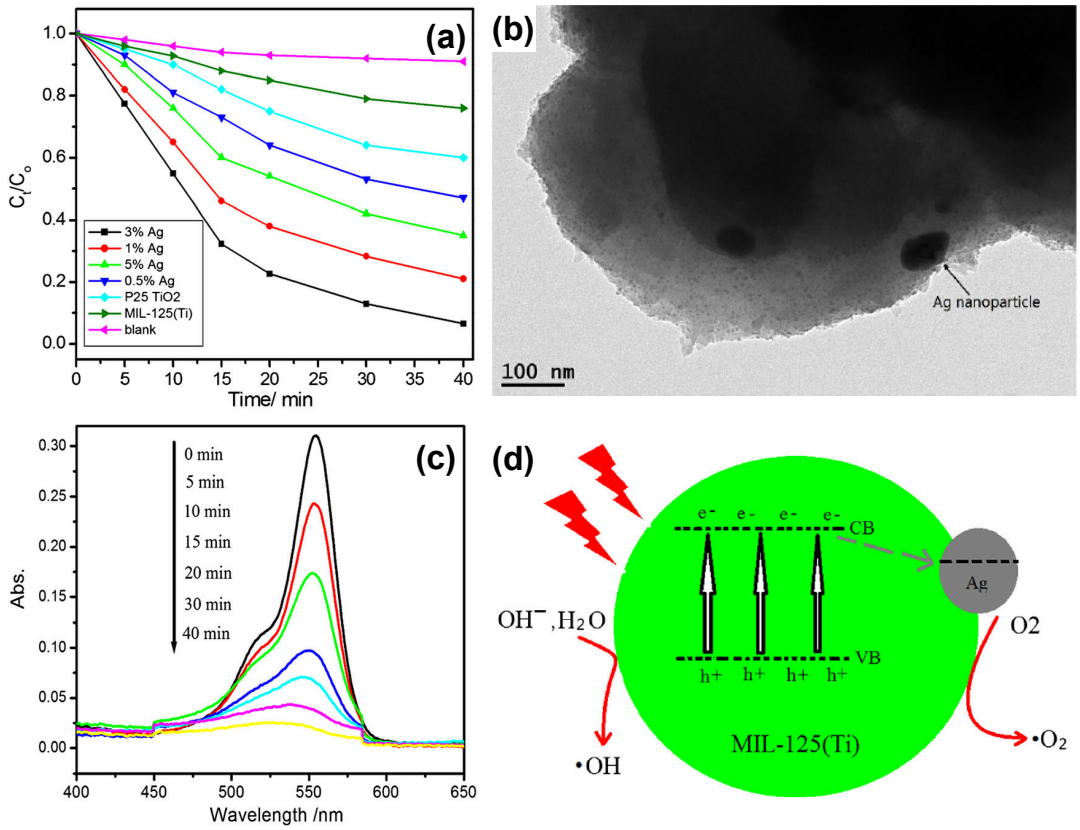


**Figure 13.** (a) Photocatalytic activity of MIL-125 and Ag/MIL-125 with various Ag loading. (b) TEM image of Ag/MIL-125 (3 wt%). (c) Absorption changes of RhB aqueous solution in the presence of Ag/MIL-125(Ti) microspheres under visible-light irradiation. (d) Possible photocatalytic mechanism of Ag/MIL-125 microspheres. Adapted with permission from Ref. [108]. Copyright 2015, John Wiley & Sons, Ltd.

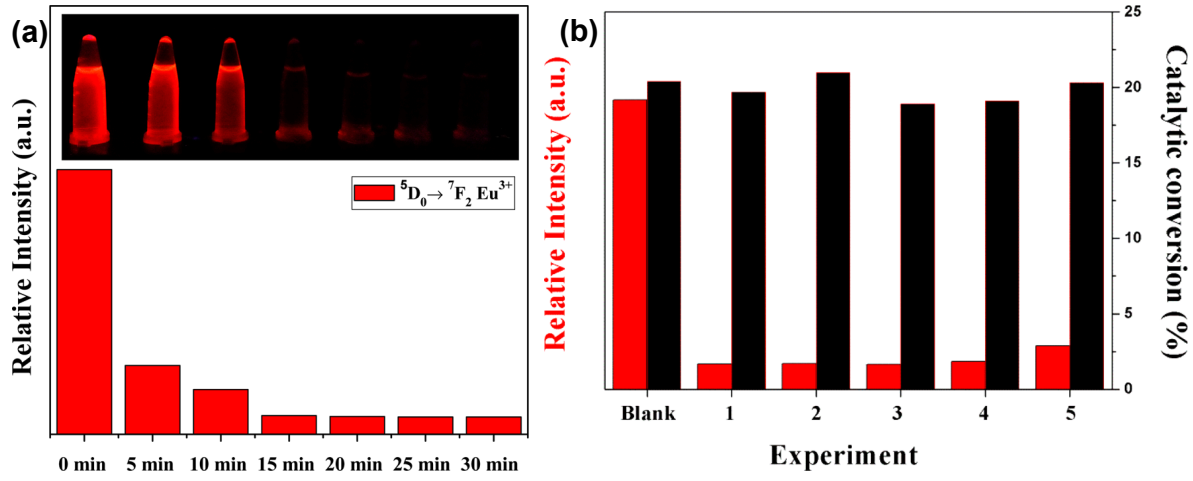


**Figure 14.** (a) Fluorescence intensity changes over time in the presence of MIL-125-AM-Eu with α-phenethyl alcohol adsorbed into channel after UV radiation. (b) Recycling experiments of MIL-125-AM-Eu for sensing α-phenethyl alcohol. Adapted with permission from Ref. [155]. Copyright 2016, American Chemical Society.

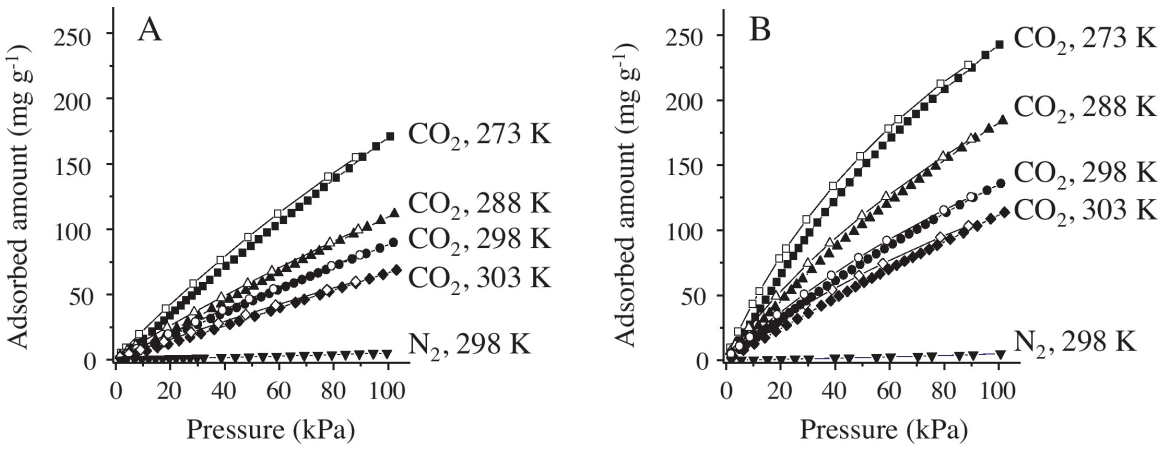


**Figure 15.** $CO_2$ and $N_2$ adsorption–desorption isotherms of (a) MIL-125 and (b) $NH_2$-MIL-125. Adapted with permission from Ref. [88]. Copyright 2012, Elsevier B.V.

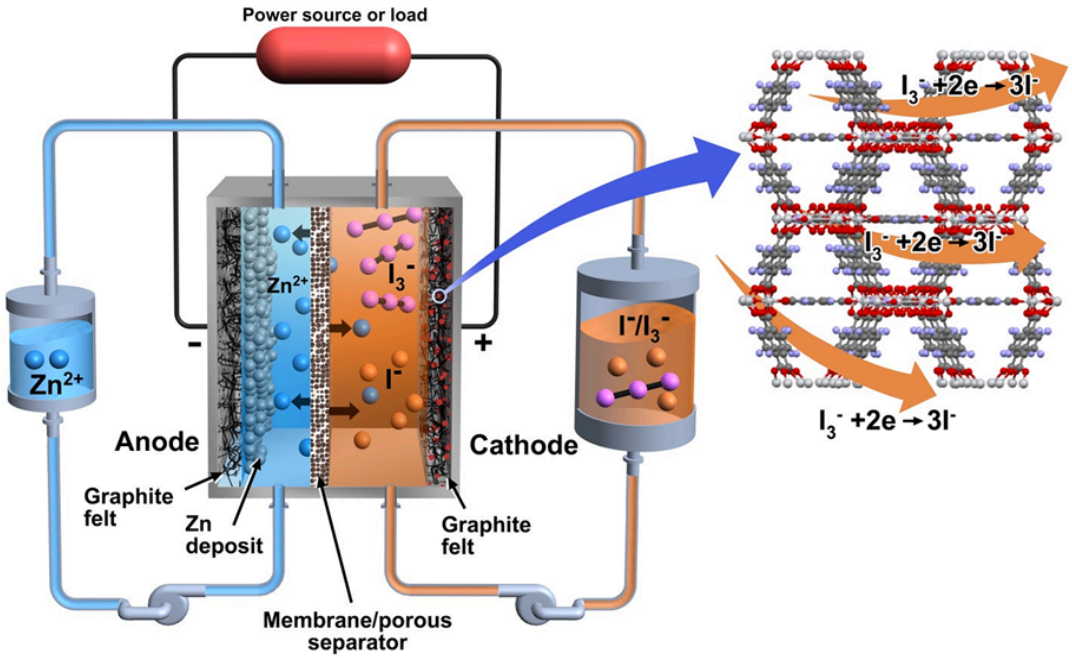


**Figure 16.** Schematic illustration of zinc-polyiodide redox flow battery with nanoporous $NH_2$-MIL-125. Adapted with permission from Ref. [164]. Copyright 2016, American Chemical Society.

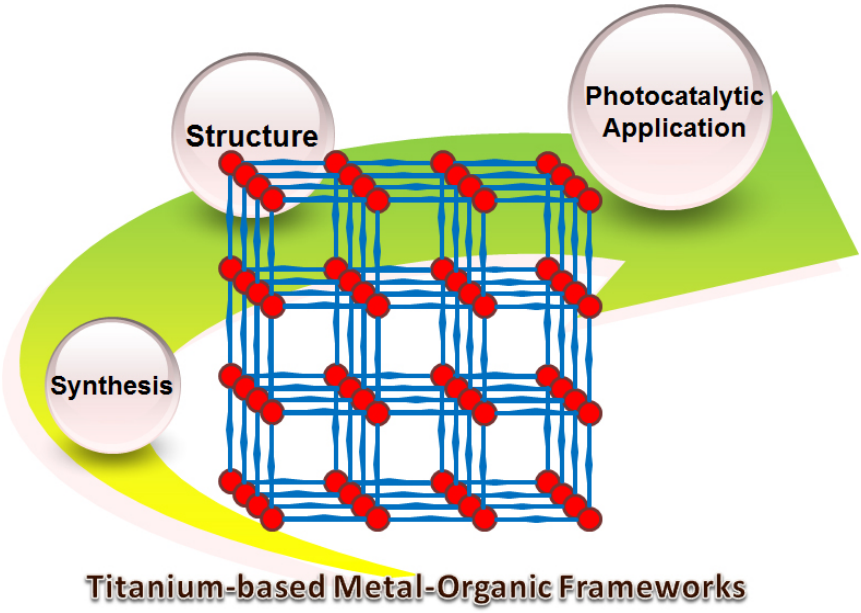


**Table of Contents Figure**